nature cancer

Article

https://doi.org/10.1038/s43018-026-01157-8

Safety and activity of RO7300490, a bispecific CD40 agonist targeted to fibroblast activation protein, in patients with advanced solid tumors: a single-arm, multicenter, first-in-human, phase 1 trial

Received: 19 December 2024

Accepted: 23 March 2026

Published online: 1 May 2026

Check for updates

A list of authors and their affiliations appears at the end of the paper

CD40 activation on dendritic cells (DCs) enhances tumor antigen cross-priming of tumor-specific cytotoxic T lymphocytes, strengthening anticancer immune responses. RO7300490 is a fibroblast activation protein (FAP)-targeted CD40 agonist antibody. In this phase I study, 80 patients with advanced and/or metastatic solid tumors received RO7300490 biweekly (dose range 16–1,100 mg). The primary objective was to evaluate safety and tolerability. Secondary/exploratory objectives included pharmacokinetics, antitumor activity and pharmacodynamics. Treatment-related adverse events (TRAEs) occurred in 53 patients (66.3%) and were mostly grade 1–2. Grade 3–4 TRAEs (3.8%) and TRAEs leading to discontinuation (2.5%) were uncommon. No grade 5 TRAEs were reported. RO7300490 showed target-mediated drug disposition, with sustained exposure at higher doses. No objective responses and limited clinical activity (disease control rate 42.5%) were observed despite rapid and persistent tumor uptake of radiolabeled RO7300490. Intratumoral pharmacodynamic activity was demonstrated by a significant increase in DC-LAMP$^+$ DC density in paired tumor biopsies. An increase in B cell density was also observed, along with the formation of pretertiary lymphoid structures, co-organized in focal micro-neighborhoods with DCs. In summary, treatment with a tumor-targeted CD40 agonist antibody is feasible, clinically manageable and induces immunomodulation of the tumor microenvironment. ClinicalTrials.gov registration: NCT04857138.

CD40 is expressed on antigen-presenting cells (APCs; dendritic cells (DCs), macrophages and B cells) and plays a central role in humoral and cellular immune responses[1]. CD40 activation is a promising approach for enhancing anticancer immunity[2], and several CD40 agonistic monoclonal antibodies have been evaluated clinically[3]; however, high rates of cytokine release syndrome (CRS), hepatotoxicity and thromboembolic events due to on-target, off-tumor CD40 activation have hampered their development[4–9]. Notably, the therapeutic window of CD40 agonists has been too narrow, resulting in only minor clinical effects, even in combination[10–12]. Fibroblast activation protein α (FAP) is expressed on a prominent fraction of cancer-associated fibroblasts and displays limited healthy tissue expression, identifying FAP as an actionable target for anticancer immunotherapies[13–16]. FAP is also associated with protumor inflammation and suppression of innate and adaptive antitumor immunity, and its expression inversely correlates with prognosis[17,18].

e-mail: bernhard.reis@roche.com

Table 1 | Patient characteristics

	All doses (*N*=80)	16 mg (*n*=6)	48 mg (*n*=4)	140 mg (*n*=27)	280 mg (*n*=7)	550 mg (*n*=32)	1,100 mg (*n*=4)
Age, years, median (range)	62.5 (35–77)	67.5 (46–77)	55.5 (35–56)	64 (42–77)	57 (46–75)	63 (40–75)	62 (53–69)
Female	28 (35.0)	4 (66.7)	1 (25.0)	12 (44.4)	2 (28.6)	9 (28.1)	0
Male	52 (65.0)	2 (33.3)	3 (75.0)	15 (55.6)	5 (71.4)	23 (71.9)	4 (100)
ECOG performance status = 0	37 (46.3)	1 (16.7)	3 (75.0)	18 (66.7)	2 (28.6)	11 (34.4)	2 (50.0)
ECOG performance status = 1	43 (53.8)	5 (83.3)	1 (25.0)	9 (33.3)	5 (71.4)	21 (65.6)	2 (50.0)
Previous LoT since diagnosis							
One	4 (5.0)	0	0	3 (11.1)	0	1 (3.1)	0
Two	19 (23.8)	0	1 (25.0)	7 (25.9)	3 (42.9)	6 (18.8)	2 (50.0)
Three	26 (32.5)	4 (66.7)	1 (25.0)	11 (40.7)	1 (14.3)	8 (25.0)	1 (25.0)
More than three	31 (38.8)	2 (33.3)	2 (50.0)	4 (22.2)	3 (42.9)	17 (53.1)	1 (25.0)
CPI experienced	65 (81.3)	4 (66.7)	3 (75.0)	23 (85.2)	6 (85.7)	25 (78.1)	4 (100)
Progressed on the last LoT before enrollment	73 (91.3)	5 (83.3)	3 (75.0)*	24 (88.9)*	6 (85.7)	31 (96.9)*	4 (100)
Unresponsive (SD) to the last LoT before enrollment	4 (5)	1 (16.7)	0	1 (3.7)	1 (14.3)	0	0
Non-small cell lung cancer	19 (23.8)	-	1 (25.0)	8 (29.6)	2 (28.6)	6 (18.8)	2 (50.0)
Mesothelioma	14 (17.5)	2 (33.3)	-	7 (25.9)	-	5 (15.6)	-
Cervical squamous cell carcinoma	7 (8.8)	2 (33.3)	-	2 (7.4)	1 (14.3)	2 (6.3)	-
Triple negative breast cancer	7 (8.8)	1 (16.7)	-	3 (11.1)	-	3 (9.4)	-
Hepatocellular carcinoma	7 (8.8)	-	-	3 (11.1)	1 (14.3)	2 (6.3)	1 (25.0)
Head and neck squamous cell carcinoma	4 (5)	-	-	-	-	4 (12.5)	-
Cutaneous melanoma	5 (6.3)	-	1 (25.0)	-	1 (14.3)	3 (9.4)	-
Urothelial cancer	4 (5.0)	-	-	1 (3.7)	-	3 (9.4)	-
Small cell lung cancer	4 (5.0)	-	-	1 (3.7)	-	3 (9.4)	-
Esophageal squamous cell carcinoma	2 (2.5)	-	-	1 (3.7)	-	-	1 (25)
Other	7 (8.8)	1 (16.7)	2 (50.0)	1 (3.7)	2 (28.6)	1 (3.1)	-
Progressed on the last LoT before enrollment	73 (91.3)	5 (83.3)	3 (75.0)*	24 (88.9)*	6 (85.7)	31 (96.9)*	4 (100)
Unresponsive (SD) to the last LoT before enrollment	4 (5)	1 (16.7)	0	1 (3.7)	1 (14.3)	0	0
Non-small cell lung cancer	19 (23.8)	-	1 (25.0)	8 (29.6)	2 (28.6)	6 (18.8)	2 (50.0)
Mesothelioma	14 (17.5)	2 (33.3)	-	7 (25.9)	-	5 (15.6)	-
Cervical squamous cell carcinoma	7 (8.8)	2 (33.3)	-	2 (7.4)	1 (14.3)	2 (6.3)	-
Triple negative breast cancer	7 (8.8)	1 (16.7)	-	3 (11.1)	-	3 (9.4)	-
Hepatocellular carcinoma	7 (8.8)	-	-	3 (11.1)	1 (14.3)	2 (6.3)	1 (25.0)
Head and neck squamous cell carcinoma	4 (5)	-	-	-	-	4 (12.5)	-
Cutaneous melanoma	5 (6.3)	-	1 (25.0)	-	1 (14.3)	3 (9.4)	-
Urothelial cancer	4 (5.0)	-	-	1 (3.7)	-	3 (9.4)	-
Small cell lung cancer	4 (5.0)	-	-	1 (3.7)	-	3 (9.4)	-
Esophageal squamous cell carcinoma	2 (2.5)	-	-	1 (3.7)	-	-	1 (25)
Other	7 (8.8)	1 (16.7)	2 (50.0)	1 (3.7)	2 (28.6)	1 (3.1)	-

Data are presented as *n* (%) unless otherwise stated. In total, 80 patients were enrolled in 6 dose-escalation cohorts (16–1,100 mg, *n*=29), 2 backfill cohorts (140 mg and 550 mg, *n*=19 and *n*=24, respectively) and 2 imaging cohorts with [^{89}Zr]Zr-RO7300490 (140 mg and 550 mg, *n*=4 each; all 8 patients received regular RO7300490 dosing after they completed the one-cycle imaging assessment). For the analyses, data from all patients were pooled based on the patient's assigned dose level (corresponding to the effective dose level received on cycle 1 day 1), irrespective of the cohort in which the patient was enrolled or intra-patient dose escalation. *Disease status previous enrollment unknown for 1 patient each in the 48 mg and 550 mg cohorts, and 2 patients in the 140 mg cohort. ECOG, Eastern Cooperative Oncology Group; LoT, line of therapy.

RO7300490 is a bispecific, FAP-targeted, CD40 (FAP-CD40) agonist antibody[19], engineered to exert CD40 agonism only when crosslinked to FAP-expressing cancer-associated fibroblasts in the tumor stroma of most human epithelial malignancies[20]. Tumor targeting is a key improvement over earlier CD40 agonists, considering the broad expression pattern of CD40 (ref. 21).

The most relevant targets for RO7300490-mediated activation in cancer immunotherapy are conventional type 1 DCs (cDC1) and DC-lysosomal associated membrane protein-positive (DC-LAMP$^+$) DCs. The cDC1 subset has high capacity for antigen cross-presentation to CD8$^+$ cytotoxic T lymphocytes (CTLs)[22,23]. Indeed, cDC1s have been described as the most potent APCs due to their CTL activation

Table 2 | Patient exposure and disposition

	All doses (*N*=80)	16 mg (*n*=6)	48 mg (*n*=4)	140 mg (*n*=27)	280 mg (*n*=7)	550 mg (*n*=32)	1,100 mg (*n*=4)
Treatment duration, median days (min–max)	54.5 (1–374)	47.5 (16–71)	71.5 (57–199)	78 (1–374)	43 (1–155)	43 (1–255)	36 (29–127)
Number of cycles, median (min–max)	4 (1–25)	3.5 (2–6)	6 (5–15)	6 (1–25)	4 (1–11)	4 (1–13)	3.5 (3–9)
Total cumulative dose, median mg (min–max)	1,190 (32–12,645)	56 (32–96)	288 (240–1,876)	840 (140–10,610)	1,120 (280–3,890)	2,200 (550–12,645)	3,850 (3,300–9,900)
Number of participants who discontinued treatment	80 (100)	6 (100)	4 (100)	27 (100)	7 (100)	32 (100)	4 (100)
Reason for discontinuation							
Progressive disease	60 (75.0)	3 (50.0)	4 (100)	21 (77.8)	3 (50.0)	26 (81.3)	3 (75.0)
Symptomatic deterioration	10 (12.5)	1 (16.7)	0	4 (14.8)	2 (28.6)	3 (9.4)	0
Adverse event	4 (5.0)	1 (16.7)	0	0	1 (14.3)	1 (3.1)	1 (25.0)
Lack of efficacy	1 (1.3)	0	0	0	0	1 (3.1)	0
Withdrawal by participant	3 (3.8)	1 (16.7)	0	1 (3.7)	0	1 (3.1)	0
Other	2 (2.5)	0	0	1 (3.7)	1 (14.3)	0	0

Data are presented as *n* (%) unless otherwise specified. Seven patients were dose-escalated during study treatment (1 patient each in the 16 mg, 280 mg and 550 mg dose levels; 4 patients in the 140 mg dose level). Twelve patients were treated beyond initial evidence of disease progression until progression was confirmed at the next assessment (1 patient each in the 16 mg and 280 mg dose levels; 2 patients each in the 48 mg and 550 mg dose levels; 6 patients in the 140 mg dose level). For the analysis, data from all patients were pooled based on the patient's assigned dose level (corresponding to the effective dose level received on cycle 1 day 1), irrespective of the cohort in which the patient was enrolled or intra-patient dose escalation.

potential[24,25]. Mice lacking cDC1 cells cannot mount CTL responses[26] and immunotherapy with checkpoint inhibitors (CPIs) is ineffective in such mice[27,28]. DC maturation/activation is essential for effective antigen cross-presentation and $CD8^+$ T cell cross-priming[29]. Moreover, the abundance of cDC1 and DC-LAMP$^+$ DCs subsets in tumor biopsies has been associated with improved prognosis and outcomes in cancer immunotherapy, supporting their importance in immune cell-mediated antitumor responses[22,30], including more prominent infiltration by $CD8^+$ T cells[31]. CD40 agonists also activate B cells, whose function in antitumor immunity is the subject of intense research as part of intratumor tertiary lymphoid structures (TLSs)[32].

By preferentially targeting tumor-infiltrating DCs, RO7300490 aims to enhance their maturation/activation, resulting in increased CTL cross-priming against tumor antigens. Data in mice bearing syngeneic tumors show antitumor activity and evidence of targeted remodeling of the tumor microenvironment (TME) in a FAP-dependent fashion[19]. Here, we report results from an open-label, first-in-human, phase I study that evaluated RO7300490 in patients with advanced and/or metastatic solid tumors.

Results

Patient characteristics and treatment exposure

Eighty patients were enrolled across ten sites within five countries (Denmark, France, Spain, Republic of Korea and the United Kingdom) between May 2021 and January 2023 to receive intravenous RO7300490 (dose range 16–1,100 mg) biweekly (Q2W). Baseline characteristics are presented in Table 1. Non-small cell lung cancer (NSCLC; 23.8%) and mesothelioma (17.5%) were the dominant indications. Most patients had received three or more lines of previous therapy (71.3%), had been exposed to ≥1 CPI (81.3%) and had progressive disease (PrD) before enrollment. Median treatment duration across all dose levels was 54.5 days (1–374 days) (Table 2). All patients had discontinued treatment at the time of this analysis, mainly due to PrD (75%) or symptomatic deterioration (12.5%).

Safety

Treatment-related adverse events (TRAEs) occurred in 53 of 80 patients (66.3%) (Table 3). Arthralgia (25 of 80; 31.3%) and asthenia (11 of 80; 13.8%) were the only TRAEs reported in ≥10% of patients; all events were grade 1–2, with no apparent dose relation. CRS (4 of 80; 5%) and infusion-related reactions (IRRs; 2 of 80; 2.5%) were all grade 1–2 and manageable. Most patients had no change in neutrophil or platelet counts (72 of 76 (94.8%) and 68 of 78 (87.2%), respectively). No adverse events (AEs) related to radiolabeled RO7300490 were reported.

Five grade 3–4 TRAEs occurred in three patients (3.8%); four were transient liver function test elevations (grade 3 alanine aminotransferase (ALT) increased, grade 3 γ-glutamyltransferase increased and grade 4 ALT/aspartate aminotransferase (AST) increased). The fifth TRAE was a grade 3 acute myocardial infarction (AMI). During percutaneous coronary intervention (PCI), diffuse narrowing of coronary arteries with no plaques or thrombi was observed.

No grade 5 TRAEs were reported. Two patients (2.5%) withdrew from treatment due to TRAEs (grade 2 drug hypersensitivity event associated with elevated IgE level and antidrug antibody (ADA) formation; grade 3 AMI).

No dose-limiting toxicities (DLTs) occurred during dose-escalation up to 1,100 mg, and the maximum tolerated dose (MTD) was not identified. However, following completion of dose escalation, a patient in the 140 mg backfill cohort had two TRAEs (grade 4 ALT/AST increased) meeting the definition of DLTs. Both events recovered with corticosteroids and did not recur after RO7300490 rechallenge.

Efficacy

Among 73 efficacy-evaluable patients, no objective clinical responses were observed per Response Evaluation Criteria in Solid Tumors (RECIST) version 1.1 (Fig. 1a). The disease control rate (DCR) was 42.5% (95% confidence interval (CI): 30.97–54.59) (Table 4). Median progression-free survival (PFS) was 50 days (95% CI: 45–85). DCR and PFS did not differ between dose levels. Fifteen of 31 patients whose best overall response (BOR) was stable disease (SD) remained stable for ≥12 weeks (Fig. 1b), and all but one had received CPIs. Exploratory analyses based on previous CPI exposure or number of previous lines of anticancer therapies did not reveal differences in DCR or PFS between subgroups (Supplementary Table 1).

Pharmacokinetics and immunogenicity

Target-mediated drug disposition (TMDD) and sustained exposure were observed at higher doses of RO7300490 (Extended Data Fig. 1a). RO7300490 pharmacokinetics (PK) was well described by a TMDD population PK model. Volume of distribution (3.17 l, relative standard error (RSE) 3.53%) from the central compartment approximated plasma volume. Clearance (0.0183 l h^{-1}, RSE 8.74%) seemed to be higher than that

https://doi.org/10.1038/s43018-026-01157-8

Table 3 | Safety summary

	All doses (*N*=80)	16 mg (*n*=6)	48 mg (*n*=4)	140 mg (*n*=27)	280 mg (*n*=7)	550 mg (*n*=32)	1,100 mg (*n*=4)
Participants with at least one AE							
AE	79 (98.8)	6 (100)	4 (100)	27 (100)	7 (100)	31 (96.9)	4 (100)
Treatment-related	53 (66.3)	3 (50.0)	3 (75.0)	16 (59.3)	5 (71.4)	23 (71.9)	3 (75.0)
Grade 3–4 AE	31 (38.8)	2 (33.3)	0	11 (40.7)	5 (71.4)	12 (37.5)	1 (25.0)
Treatment-related	3 (3.8)	1 (16.7)	0	3 (3.7)	1 (14.3)	0	0
Serious AE	28 (35.0)	2 (33.3)	0	10 (37.0)	6 (85.7)	9 (28.1)	1 (25.0)
Treatment-related	5 (6.3)	0	0	3 (11.1)	1 (14.3)	1 (3.1)	0
Grade 5 (fatal) AE	1 (1.3)	0	0	0	0	0	1 (1.3)
Treatment-related	0	0	0	0	0	0	0
AE leading to treatment withdrawal	4 (5.0)	1 (16.7)	0	0	1 (14.3)	1 (3.1)	1 (25.0)
Treatment-related	2 (2.5)	1 (16.7)	0	0	1 (14.3)	0	0
AE leading to dose interruption	28 (35.0)	2 (33.3)	0	13 (48.1)	3 (42.9)	9 (28.1)	1 (25.0)
DLT	1 (1.3)	0	0	1 (3.7)	0	0	0
IRR/CRS/hypersensitivity	7 (8.8)	1 (16.7)	0	1 (3.7)	1 (14.3)	4 (12.5)	0
ImAE requiring corticosteroid use	5 (6.3)	1 (16.7)	0	2 (7.4)	0	1 (3.1)	1 (25.0)
Participants with at least one TRAE with occurrence rate ≥10%							
Arthralgia	25 (31.3)	0	2 (50.0)	7 (25.9)	2 (28.6)	12 (37.5)	2 (50.0)
Grade 1–2	25 (31.3)	0	2 (50.0)	7 (25.9)	2 (28.6)	12 (37.5)	2 (50.0)
Grade ≥3	0	0	0	0	0	0	0
Asthenia	11 (13.8)	2 (33.3)	0	2 (7.4)	0	6 (18.8)	1 (25.0)
Grade 1–2	11 (13.8)	2 (33.3)	0	2 (7.4)	0	6 (18.8)	1 (25.0)
Grade ≥3	0	0	0	0	0	0	0
Number of participants with total neutrophils (Abs) grade change post-baseline							
Total	76	5	3	26	7	31	4
No change	72 (94.7)	5 (100)	3 (100)	25 (96.2)	6 (85.7)	30 (96.8)	3 (75)
Grade 1	2 (2.6)	0	0	1 (3.8)	1 (14.3)	0	0
Grade 3	1 (1.3)	0	0	0	0	1 (3.2)	0
Missing	1 (1.3)	0	0	0	0	0	1 (25)
Number of participants with platelets (Abs) grade change post-baseline							
Total	78	6	4	26	7	31	4
No change	68 (87.2)	6 (100)	2 (50)	24 (92.3)	7 (100)	26 (83.9)	3 (75)
Grade 1	10 (12.8)	0	2 (50)	2 (7.7)	0	5 (16.1)	1 (25)

Data are presented as *n* (%). All participants enrolled in the study received at least one dose of RO7300490 and were evaluable for safety. For the analysis, data from all patients were pooled based on the patient's assigned dose level (corresponding to the effective dose level received on cycle 1 day 1). Abs, absolute; ImAE, immune-mediated adverse event.

of a typical IgG1 antibody. Steady-state median concentrations were 6.56 and 64.5 μg ml^{-1} for 140 and 550 mg Q2W, respectively. Median receptor occupancy (RO; saturation of the target-mediated clearance) derived from the TMDD population PK model for 140 and 550 mg Q2W was 30.3% and 87.6%, respectively (Extended Data Fig. 1b). Median time above 80% RO was 0.83 days (20 h) and 11.8 days, respectively. Saturation of the target-mediated clearance and sustained serum exposure during the entire dosing interval was reached at doses ≥550 mg, with RO7300490 displaying a half-life of 7 days.

Pre-existing ADAs against RO7300490 were detected in 3 of 80 (3.8%) patients before treatment, while 8 of 75 immunogenicity-evaluable patients developed ADAs during treatment (ADA incidence 10.7%). None of these patients was reported as treatment-enhanced ADA positive. Given the sparse data and low occurrence of ADAs, their effect on the PK of RO7300490 could not be assessed. Excluding one patient who developed IgE-mediated drug hypersensitivity associated with ADA formation, no apparent impact of ADAs was observed on the safety profile of the other ADA-positive patients.

Tumor uptake

Despite considerable inter- and intra-patient variability, [^{89}Zr]Zr-RO7300490 uptake in tumor lesions of patients treated with the 140 mg labeled dose was detectable. Signals appeared 24 h post-infusion and displayed a best signal-to-background contrast after 96 h (Fig. 2a and Extended Data Fig. 2). [^{89}Zr]Zr-RO7300490 tumor uptake in patients treated with the 550 mg labeled dose was generally weaker, and occasionally not visible above background. A moderate signal was detected in healthy liver and spleen, which are highly perfused organs with high CD40 expression. Liver uptake and colon signals observed in some cases were consistent with hepatobiliary clearance of radiolabeled antibodies[33]. Median [^{89}Zr]Zr-RO7300490 tumor-to-blood ratio (TBR) for the 140 mg dose 24 h post-infusion was 0.87, rising to 2.5 and 5.3 after 96 and 168 h, respectively (Fig. 2b). At the 550 mg dose, tumor uptake was lower with median TBR of 0.51, 0.97 and 1.6 at 24, 96 and 168 h post-infusion, respectively, suggesting that RO7300490 binding sites become saturated with excess unlabeled RO7300490 co-administered with the trace amount of [^{89}Zr]Zr-RO7300490.

https://doi.org/10.1038/s43018-026-01157-8

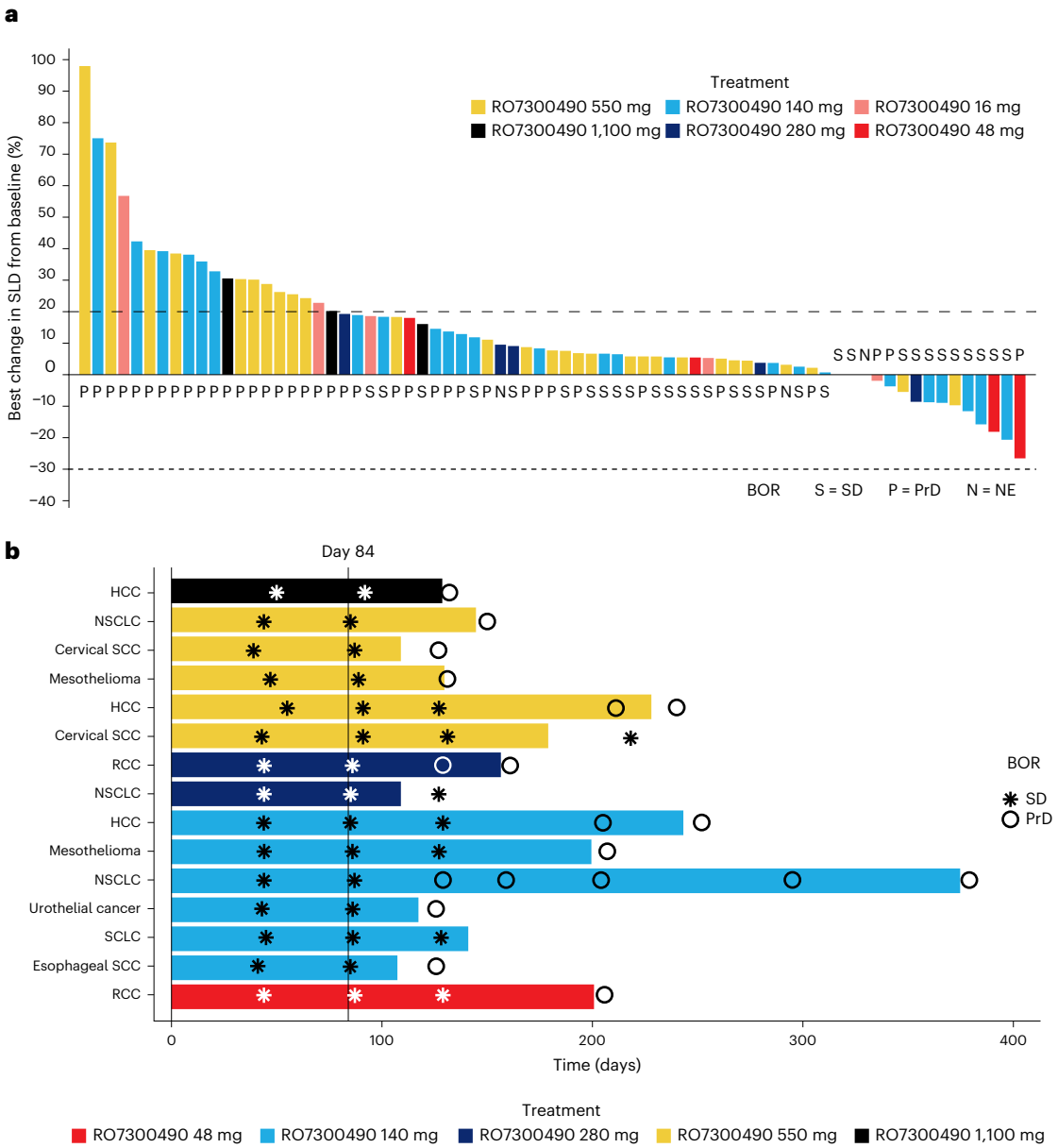

Fig. 1 | Clinical activity. a, Best changes from baseline in the sum of the long diameters (SLD) of the target lesions for 73 patients who were evaluable for efficacy are shown. Each bar represents the results from an individual patient, and is color-coded according to the first dose of RO7300490 received. The patient's BOR is indicated under or above each bar. **b**, Swimmer plot of 15 patients who remained in SD (15 of 31) for ≥12 weeks. Cancer types are indicated on the *y* axis. Bars represent the duration of study treatment from the first dose to the last dose of RO7300490. Three patients discontinued study treatment for other reasons than PrD (AE, symptomatic deterioration, lack of efficacy). NE, not evaluable; HCC, hepatocellular carcinoma; RCC, renal cell carcinoma; SCC, squamous cell carcinoma; SCLC, small cell lung cancer.

These findings demonstrate that RO7300490 accumulates within the tumor tissue and that CD40 engagement is saturated at 550 mg.

Peripheral saturation of CD40 binding sites

CD40 RO on circulating lymphocytes was measured to assess RO7300490 binding to CD40 (peripheral sink). At the lowest dose, RO on B cells reached 100% within 24 hours post-infusion before rapidly declining to undetectable levels within 7 days (Extended Data Fig. 3a). High RO persisted longer as RO7300490 doses increased, remaining at 100% over the entire treatment cycle at doses ≥280 mg. The dose-dependent RO kinetics on monocytes was similar to that seen on B cells (Extended Data Fig. 3b). CD40 RO data were consistent with the TMDD-derived RO from PK measurements and TMDD population PK modeling (Extended Data Fig. 1b), indicating full saturation of the peripheral receptor sink at ≥550 mg over the dosing interval.

Limited RO7300490 peripheral pharmacodynamic effects

RO7300490 led to a marked, dose-dependent reduction of B cell count during the first cycle, down by approximately 90% compared to pre-dose levels at the highest dose tested (1,100 mg) (Extended Data Fig. 3c). B cell count recovery before the next dose administration was dose-dependent at lower doses, but remained suppressed throughout each cycle at doses ≥140 mg. A trend toward B cell count recovery in later cycles was observed.

RO7300490 did not result in significant elevation of circulating cytokines (Extended Data Fig. 3d). There was a minor trend for CXCL10 and interleukin (IL)-6 increase at doses >280 mg; maximum

Table 4 | Summary of efficacy

	All doses (*N*=73)	16 mg (*n*=5)	48 mg (*n*=4)	140 mg (*n*=26)	280 mg (*n*=5)	550 mg (*n*=29)	1,100 mg (*n*=4)
Overall response rate, %	0	0	0	0	0	0	0
DCR, *n* (%) 95% CI	31 (42.5) 31.0–54.6	2 (40.0) 5.3–85.3	2 (50.0) 6.8–93.2	13 (50.0) 29.9–70.1	3 (60.0) 14.7–94.7	10 (34.5) 17.9–54.3	1 (25) 0.6–80.6
PFS in days, median (95% CI)	50 (45–85)	50 (44–NE)	64 (43–NE)	80.5 (45–89)	85 (23–NE)	46 (43–86)	88 (37–NE)
Complete response	0	0	0	0	0	0	0
Partial response	0	0	0	0	0	0	0
SD SD ≥12 weeks	31 (42.5) 15 (20.5)	2 (40.0) 0	2 (50.0) 1 (25.0)	13 (50.0) 6 (23.1)	3 (60.0) 2 (40.0)	10 (34.5) 5 (17.2)	1 (25.0) 1 (25.0)
Progressive disease	39 (53.4)	3 (60.0)	2 (50.0)	13 (50.0)	1 (20.0)	18 (62.1)	2 (50.0)
NE	3 (4.1)	0	0	0	1 (20.0)	1 (3.4)	1 (25.0)

Data are presented as *n* (%) unless otherwise specified. Seventy-three patients received at least one dose of RO7300490 and had at least one post-baseline tumor assessment after 6 weeks or discontinued the study due to symptomatic deterioration and were included in the efficacy-evaluable population.

peak concentrations remained within the range of natural biological variability. Soluble CD25 concentrations were not altered by RO7300490. No signs of peripheral lymphocyte activation were apparent, except for reduced B cell counts, in line with preclinical data and the tumor-targeted mechanism of action (MOA)[10].

Increased tumor DC-LAMP$^+$ DC density and activation

Immunofluorescence (IF) image analysis from biopsies collected at baseline and on-treatment revealed a significantly higher tumor tissue density of total DC-LAMP$^+$ DCs, and DC-LAMP$^+$ DCs coexpressing the activation markers CD86 or PD-L1, after RO7300490 treatment. Total DC-LAMP$^+$ DC density increased in nine of 11 samples in the 140 mg cohort ($\log_2$ fold change (FC) = 3.14, *P* value ~ 0.01, degrees of freedom (d.f.) = 10; Fig. 3a) and eight of eight samples in the 550 mg cohort ($\log_2$FC = 2.13, *P* value ≤ 0.01, d.f. = 7; Fig. 3b). CD86 + /DC-LAMP + DC density also increased following treatment at 140 mg (nine of ten samples, $\log_2$FC = 3.38, *P* value ≤ 0.01, d.f. = 9) and at 550 mg (eight of eight samples, $\log_2$FC = 3.9, *P* value ~ 0.01, d.f. = 7). Similarly, PD-L1$^+$/DC-LAMP$^+$ DCs in both cohorts increased in density (140 mg, six of seven samples, $\log_2$FC of means = 3.13, *P* value = 0.04, d.f. = 6; 550 mg: six of eight samples, $\log_2$FC = 2.38, *P* value = 0.04, d.f. = 7). These proximal pharmacodynamic (PD) effects were independent of whether the patient experienced PrD or SD as BOR (Fig. 3 and Extended Data Fig. 4).

The treatment-induced increase in the density of the DC-LAMP$^+$ DCs was clearly visible on IF images due to their scarcity in baseline biopsy samples (Fig. 3c). It was also confirmed visually that individual DC-LAMP$^+$ DCs coexpressed CD86, PD-L1 or both (Fig. 3d), suggesting these DCs represent a mature DC subpopulation, consistent with the expression of DC-LAMP and its described association with mature DCs[14]. In one case, a focal accumulation of DC-LAMP$^+$ DCs around vessels in lesions collected after treatment was noted (Fig. 3e).

Decreased tumor cDC1 density

cDC1 DC density in tumor tissue decreased after treatment in most patients. In the 140 mg cohort, a decrease was observed in eight of 12 samples ($\log_2$FC of means = −0.77, *P* value = 0.04, d.f. = 11; Fig. 3f). In the 550 mg cohort, cDC1 decrease was apparent in five of seven samples ($\log_2$FC = −2.29, *P* value = ~0.09, d.f. = 6; Fig. 3g). When both cohorts were pooled, the reduction in cDC1 density upon treatment reached statistical significance ($\log_2$FC = −1.23, *P* value ≤ 0.01, d.f. = 18).

Increased tumor B cell density and focal colocalization with DC-LAMP$^+$ DCs

Upon treatment, B cell density in tumor tissue increased in eight of 11 samples in the 140 mg cohort ($\log_2$FC = 1.4, *P* value ~ 0.1, d.f. = 10) and in five of eight samples in the 550 mg cohort ($\log_2$FC = 2.5, *P* value = 0.3, d.f. = 7) (Fig. 4a,b). Despite numerical increases, changes were not statistically significant, including in a pooled analysis ($\log_2$FC = 1.84, *P* value = 0.058, d.f. = 18). B cell activation markers were not consistently altered by treatment (Fig. 4a,b). B cell PD effects were independent of whether the patient experienced PrD or SD as BOR (Fig. 4 and Extended Data Fig. 4).

In patients with increased B cell density, the magnitude of the effect was visually striking. Figure 4c shows an increased number of enlarged B cell foci after treatment. Of note, the increased B cell foci in tissue contrast with the reduction in peripheral B cell count in blood (Extended Data Fig. 3c).

DC-LAMP$^+$ DCs were frequently colocalized in scatters or in foci together with B cells, forming small lymphocytic aggregates morphologically reminiscent of early TLS (Fig. 4d). However, the limited size of these focal structures and the absence of visible high endothelial venules led us to conclude these were not fully developed and mature TLS.

The cell density of total or activated CLEC10A$^+$ cDC2 or macrophages was not significantly altered by treatment within the tumor tissue (Extended Data Fig. 5). No changes in CD8$^+$ T cell infiltration, granzyme B effector CD8$^+$ T cells or Foxp3$^+$ regulatory T cells were observed in paired biopsies after treatment (Extended Data Fig. 6a,b).

RNA sequencing of tissue PD effects

Paired biopsies were subjected to RNA sequencing to identify treatment-induced changes in the expression of individual genes (Extended Data Fig. 7a) or sets of genes grouped by pathways using published gene signatures (Extended Data Fig. 7b). Gene expression analysis showed strong upregulation of the DC-LAMP$^+$-specific genes *CCL17* and *LAMP3* (*DC-LAMP*) (pooled analysis $\log_2$FC = 5, false discovery rate (FDR) <0.01 and $\log_2$FC = 1.2, FDR = 0.07 for *CCL17* and *LAMP3*, respectively), and induction of the activated DC-LAMP$^+$ signature cDC_CCR7 ($\log_2$FC = 1.7, FDR = 0.01). A trend was observed for induction of genes associated with B cells (*CR2* and *MS4A1*) or TLS formation (*CCL19*, *CCL21*, *CCL22* and *CXCL13*). These gene-specific changes were reflected in B cell- and TLS-specific signatures, respectively, confirming results obtained by IF analysis. RNA sequencing indicated inflammatory pathway initiation via *PTGDS* and *TNFRSF9* upregulation, whereas drug target genes (*CD40* and *FAP*) remained stable. Consistent with immunohistology, CD8/cytotoxicity genes trended downward, with CTL signatures significantly declining (0.1–0.01 FDR) in a patient subset (Extended Data Fig. 7c). Furthermore, significant reductions in macrophage genes (*C1QB*, *MS4A7* and *CD209*) and signatures suggested microenvironment remodeling.

Identifying sensitive patient population characteristics

Using hierarchical clustering on treatment-induced changes in gene expression, patients were categorized into two distinct clusters separated based on positive or negative gene regulation, regardless of

https://doi.org/10.1038/s43018-026-01157-8

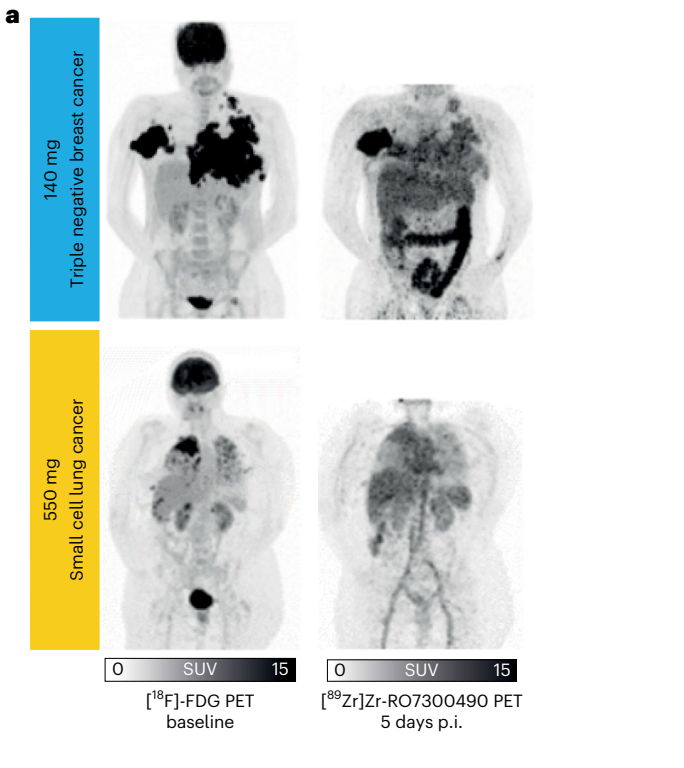

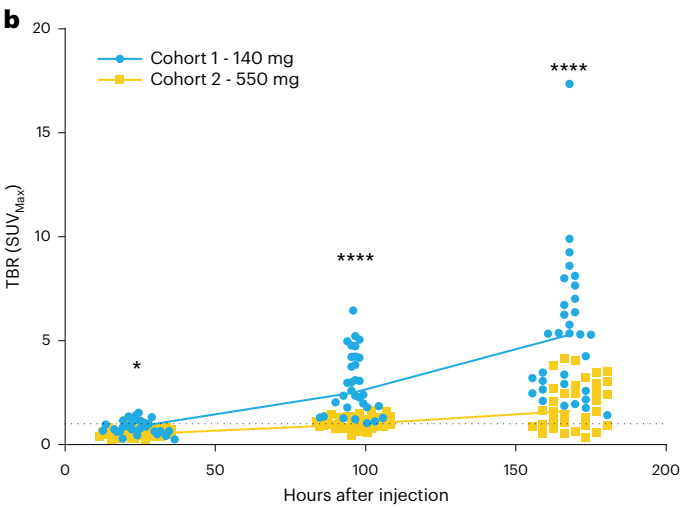

Fig. 2 | Biodistribution of RO7300490. a, Representative images of baseline FDG-PET and post-dosing [^{89}Zr]Zr-RO7300490 PET scans from 2 patients treated with an imaging dose of 140 mg or 550 mg, respectively. Darker areas indicate high radiolabeled uptake. **b**, TBR plotted over time post-dosing. In total, 65 lesions, equally distributed between the 2 imaging doses (4 patients per dose), were identified and quantified. Two-tailed *t*-test for 24 hours ($P = 0.0251$); two-tailed Mann–Whitney test for 96 hours and 168 hours (nonparametric, $P < 0.0001$ each). TBR = 1 (tumor–blood equilibrium) is indicated by the dotted line. [^{18}F]-FDG-PET, fluorodeoxyglucose-positron emission tomography; ^{89}Zr, zirconium-89; SUV_{Max}, maximum standard uptake value.

whether they received 140 or 550 mg (Extended Data Fig. 7c). Tumor samples from patients in cluster I exhibited upregulation of genes associated with DC and B cell activation, T cell activation and tumor rejection. Tumor samples from patients in cluster II exhibited a reduction in genes associated with tumor rejection (for example CD8$^+$ T cell signatures, IFNγ pathway). Using a logistic regression model for each parameter, we investigated if this dichotomous separation was associated with clinical or biomarker-derived parameters. Patients with NSCLC (all CPI-experienced) were significantly more likely to reside in the non-activated cluster II (odds ratio 0.09; $P = 0.01$). In contrast, three of three CPI-naive patients and four of five patients experiencing long SD (BOR of SD with a minimum duration of ≥12 weeks) were categorized into (activated) cluster I. Associations with CPI pretreatment and long SD did not reach statistical significance (*P* value, >0.1), possibly due to low sample numbers.

The reliability of the model prediction was assessed using a calibration plot, showing good agreement between predicted probabilities and observed outcomes, with an area under the receiver operating characteristic (ROC) curve of 0.71 (Extended Data Fig. 8).

Correlation between FAP expression and BOR or DC PD effects

The RO7300490 MOA suggests tumor stroma displaying high FAP expression would be more likely to elicit CD40 receptor crosslinking and subsequent response to treatment[19]. Although there was a trend for a higher median FAP expression in the BOR SD group, the difference versus FAP expression in the BOR PrD group was not significant ($P = 0.16$) (Extended Data Fig. 9a). When investigating association with PD effects (Extended Data Fig. 9b), a trend for a positive correlation between FAP expression and increased density in DC-LAMP$^+$ DCs was seen in both the 140 mg ($R = 0.46$, $P = 0.15$) and 550 mg cohort ($R = 0.48$, $P = 0.23$). A significant inverse correlation between FAP expression and cDC1 density was observed in the 550 mg cohort ($R = -0.85$, $P = 0.015$). Result interpretation requires caution as FAP and DC density assessments were performed on separate (non-adjacent) tissue biopsy slides, potentially confounding the analysis due to intratumoral variability. When dose cohorts were pooled, the increase in DC-LAMP$^+$ and decrease in cDC1 were significantly correlated with higher FAP expression (DC-LAMP, $R = 0.47$, $P = 0.042$; cDC1, $R = -048$, $P = 0.045$). Representative immunohistochemistry (IHC) images of FAP-positive cells in the tumor region (epithelium and stroma) of baseline samples from four patients are shown in Extended Data Fig. 9c.

Discussion

Results from this first-in-human, phase I study show that single-agent RO7300490 was well tolerated and that toxicities were manageable. Most AEs were mild-to-moderate and nonserious, including at doses demonstrating relevant exposure and proven saturation of the peripheral sink. There was no clear trend for a dose-related increase in TRAE incidence or severity. The MTD could not be identified. This therapeutic window is a marked improvement versus those achieved by conventional CD40 agonists[4,8,34], and reaches a fourfold higher safe dose than the second-generation mesothelin-targeted bispecific CD40 agonist ABBV-428 (tolerable up to 3.6 mg kg^{-1})[35]. This is further illustrated by the low incidence of CRS/IRR or decrease in white blood cell and platelet counts that are commonly associated with CD40 agonists[3,4,6–8,34]. Transient abnormalities in liver function tests indicating hepatocyte cytolysis have also been reported[4,6–8,34,35]. It has been hypothesized that hepatotoxicity might be mediated by myeloid cells[36,37] and IL-12p40 (ref. 38). Additionally, CD40$^+$ hepatocytes undergo apoptosis after CD40 activation[39]. We observed no change or mildly increased transaminases in most patients, a notable improvement versus earlier CD40 agonists. Arthralgia was the most frequent TRAE (31.3%). As FAP is overexpressed in osteoarthritic synovium[40,41], this could be an on-target, off-tumor effect of RO7300490. Of note, FAP is identified as a potential factor mediating atherosclerotic plaque instability and fibrous cap degradation[42,43]; however, no cardiovascular or cerebrovascular events were observed in studies with FAP-targeting monoclonal antibodies[15,16,44,45]. Although reported as a TRAE, the grade 3 AMI observed in one patient is unlikely to be a FAP-mediated AE. The participant had multiple cardiovascular risk factors and findings during PCI were inconsistent with the RO7300490 MOA.

A recurring challenge with targeting CD40 is its widespread expression, which impacts tolerability of CD40 agonists due to on-target,

https://doi.org/10.1038/s43018-026-01157-8

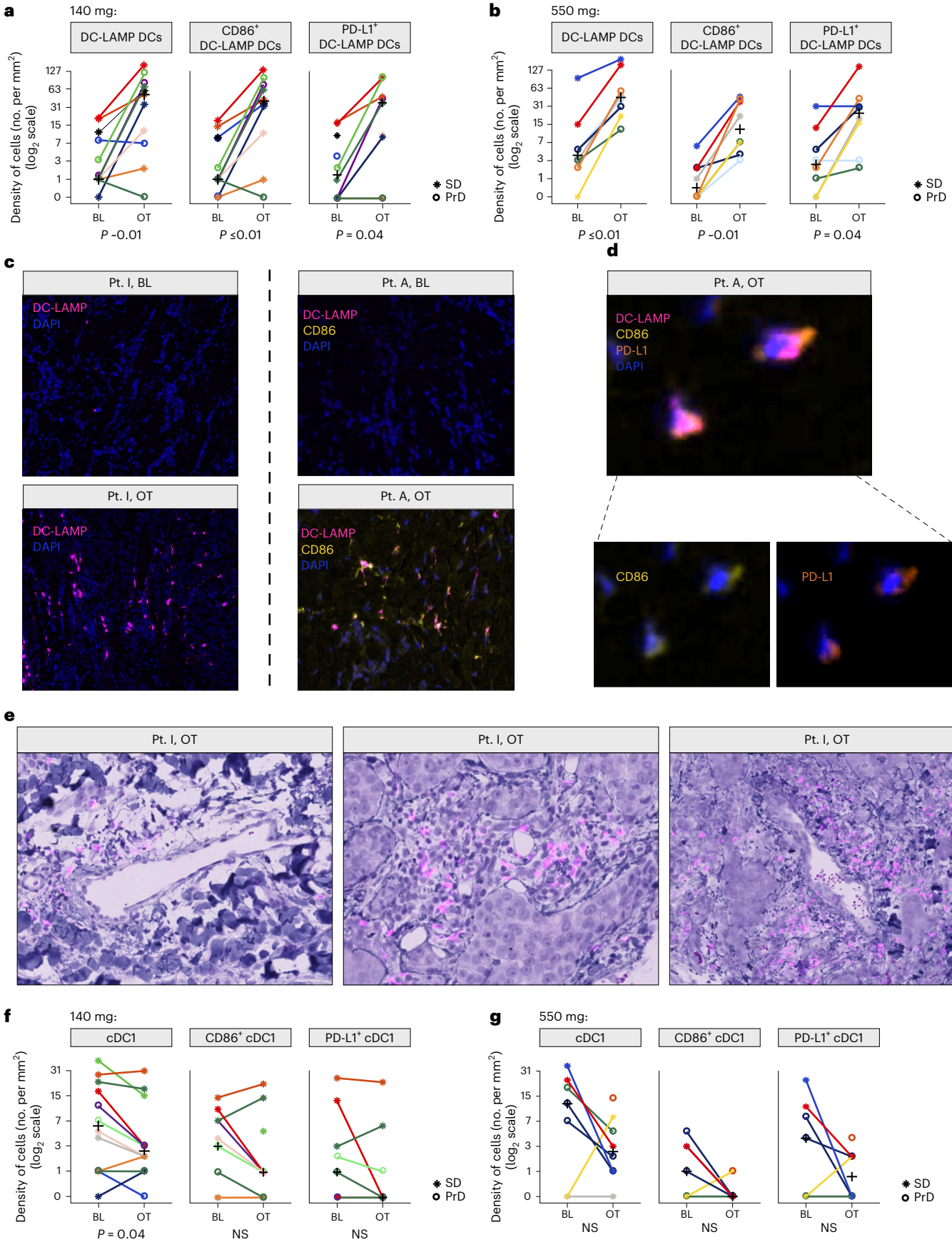

Fig. 3 | PD effects on DC subtypes in tumor. a,**b**, Infiltration and activation status (markers, CD86 and PD-L1) of mature DC-LAMP$^+$ DCs were analyzed by a multiplex-IF assay of baseline (BL) and on-treatment (OT) paired tissue biopsies at 140 mg (**a**) or 550 mg (**b**). Number of paired biopsies tested: for the density of DC-LAMP$^+$ cells, $n = 19$ (140 mg cohort $n = 11$; 550 mg cohort $n = 8$); for the CD86$^+$DC-LAMP$^+$ cells, $n = 18$ (140 mg cohort $n = 10$; 550 mg cohort $n = 8$); and for the PD-L1$^+$DC-LAMP$^+$ cells, $n = 15$ (140 mg cohort $n = 7$; 550 mg cohort $n = 8$). Infiltration was determined based on density (number of cells per mm^2 tissue) and changes were calculated based on $\log_2$FC of means. Individual patient results are differentiated by color and the cross corresponds to the median value at each time point. Labels indicate patient RECIST v.1.1 BOR. Unconnected data points: paired sample did not meet quality check criteria and was not included in the analysis. **c**, Representative multiplex-IF images from two patients (pt. I (breast cancer, skin lesion) and pt. A (mesothelioma, lung lesion)) showing DC-LAMP$^+$ density in paired BL and OT biopsy tissues. Pt. A: samples showing co-staining of DC-LAMP with CD86. At BL, no DC-LAMP and/or CD86$^+$ cells are visible. At OT, some DC-LAMP$^+$ cells (pink) are visible, and almost all were well positive for CD86 (yellow). Purple, DC-LAMP; yellow, CD86; blue, 4,6-diamidino-2-phenylindole (DAPI) (nuclei). **d**, Example showing increased magnification with co-expression of the activation markers PD-L1 and CD86 on DC-LAMP$^+$ DCs in OT biopsy tissues. Purple, DC-LAMP; yellow, CD86; orange, PD-L1; blue, DAPI (nuclei). **e**, Sample with DC-LAMP$^+$ cells focally localized around vessels. Hematoxylin and eosin (H&E) images from an OT biopsy (pt. I, breast cancer, skin lesion) capture the accumulation of DC-LAMP$^+$ DCs around vessels. DC-LAMP$^+$ cell signals are shown superimposed on top of the H&E image. **f**,**g**, Infiltration and activation status (markers, CD86 and PD-L1) of CLEC9A$^+$ cDC1 were analyzed by a multiplex-IF assay of BL and OT paired tissue biopsies at 140 mg (**f**) or 550 mg (**g**). Number of paired biopsies tested: for the total density of cDC1 cells, $n = 19$ (140 mg cohort $n = 12$; 550 mg cohort $n = 7$); for the CD86$^+$ cDC1 cells, $n = 14$ (140 mg cohort $n = 8$; 550 mg cohort $n = 6$); and for the PD-L1$^+$ cDC1 cells, $n = 12$ (140 mg cohort $n = 6$; 550 mg cohort $n = 6$). Infiltration was determined based on density (number of cells per mm^2 tissue) and changes were calculated based on $\log_2$FC of means. Individual patient results are differentiated by color and the cross corresponds to the median value at each time point. Labels indicate patient RECIST v.1.1 BOR. For **a**, **b**, **f** and **g**, patients with paired biopsies from the backfill cohorts were included in this analysis. Three patients were removed from the analysis as samples did not pass the quality control check; see Supplementary Table 5 for details. Pt, patient; NS, not significant.

off-tumor binding, and also limits their accumulation within tumor lesions. Saturation of peripheral CD40 binding sites is a likely prerequisite to allow therapeutic concentrations of RO7300490 to reach the tumor. We confirmed that RO7300490 shows a TMDD with sustained exposure at higher doses, and a half-life of 7 days at doses ≥550 mg. The sustained exposure led to persistent saturation of peripheral CD40 receptors, without triggering systemic inflammation, throughout the treatment cycle as predicted by preclinical models[19]. Saturation of the peripheral sink was further confirmed by [^{89}Zr]Zr-RO7300490-positron emission tomography (PET). These analyses also showed that tumor uptake of RO7300490 was rapid and persisted over several days. No abnormal patterns of RO7300490 accumulation in healthy tissue were seen, consistent with the observed safety profile of the molecule.

For comparison, previous CD40 agonists including mitazalimab, a CD40 agonistic monoclonal antibody under clinical development, showed half-life values between 0.5 and 1 day at the efficacious dose range of 42 to 140 mg Q2W in a phase I study[8,12]. RO7300490 could be safely explored at substantially higher doses (up to 1,100 mg Q2W); its wider therapeutic window and improved half-life allowed the testing of doses achieving transient or persistent saturation of peripheral CD40 receptors.

RO7300490 caused a marked reduction of circulating B cells, as observed with other CD40-targeting drugs[5,7,8]. RO7300490 did not trigger plasma cytokine elevations or severe CRS-related AEs, consistent with the intended design of the molecule requiring local, FAP-mediated crosslinking for activation of CD40 (ref. 19).

RO7300490 resulted in a notable increase of DC-LAMP$^+$ DC density in tumor tissue, confirming intratumoral PD activity and thereby offering a proof of mechanism. The increase in intratumoral DC-LAMP$^+$ DCs was consistently detected by IF and RNA sequencing. In parallel, a decrease in cDC1 density to almost undetectable levels was observed. This could be explained by overactivation causing cell demise, outmigration toward tumor-draining lymph nodes, differentiation into more mature DCs or a combination of these. The intratumoral density increase of DC-LAMP$^+$ DCs and the concurrent decrease of cDC1 precursor cells suggests CD40 crosslinking directly or indirectly induced cDC1 differentiation toward DC-LAMP$^+$ DCs. This is consistent with literature reporting that mature DC-LAMP$^+$ DCs can develop from both cDC1 or cDC2 DCs, retaining the respective functional properties of their precursor cells[46]. The magnitude of the PD effects on both DC subtypes correlated with FAP expression levels in tumor stroma, emphasizing the local, tumor-targeted MOA of RO7300490 and its specific biological activity on cells expressing high CD40 receptor levels.

DC-LAMP$^+$ DCs are associated with TLS formation and B cell infiltration in the tumor[47–50]. In many patients, RO7300490 led to a notable increase in intratumor density and formation of pre-TLS, co-organized in focal micro-neighborhoods together with DC-LAMP$^+$ DCs coexpressing activation markers. These observations strongly suggest that DC-LAMP$^+$ DCs induced by RO7300490 assume an active, immunomodulatory role in crosstalk with proliferating B cells. Previous reports have also implicated CD40 signaling with the induction of TLS[51,52]. Of note, intratumoral injection of an Fc-optimized agonist anti-CD40 mAb into superficial tumors demonstrated DC activation and TLS formation, consistent with our findings[53].

Although CD40 engagement by RO7300490 leads to local immunomodulation of the TME, it displayed limited clinical activity in our study when administered as a single agent. Induction of regulatory T cells by DC-LAMP$^+$ DCs is an unlikely explanation, as their numbers did not change upon treatment. Consistent with the lack of evidence for single-agent efficacy is the absence of CD8 infiltration and T cell activation, a finding that was not unexpected in patients with solid tumors who have progressed on prior treatments, including CPIs[54,55]. Some patients who progressed on their previous line of therapy experienced prolonged SD, which has been associated with better overall survival in several solid tumors following different treatments[56,57]. Rational combinations seeking synergy include CPIs, but also other experimental agonists or cancer vaccines.

Fig. 4 | PD effects on tumor B cells and DC-B cell interactions. a,**b**, Infiltration and activation status (markers, CD86 and PD-L1) of CD20$^+$ B cells were analyzed by a multiplex-IF assay of BL and OT paired tissue biopsies at 140 mg (**a**) or 550 mg (**b**). Patients with paired biopsies from the backfill cohorts were included in this analysis. Three patients were removed from the analysis as samples did not pass the quality control check; see Supplementary Table 5 for details. Number of paired biopsies tested: for the total density of B cells, $n = 19$ (140 mg cohort $n = 11$; 550 mg cohort $n = 8$); for the CD86$^+$ B cells, $n = 16$ (140 mg cohort $n = 8$; 550 mg cohort $n = 8$); and for the PD-L1$^+$ B cells, $n = 15$ (140 mg cohort $n = 7$; 550 mg cohort $n = 8$). Infiltration was determined based on density (number of cells per mm^2 tissue) and changes were calculated based on $\log_2$FC of means. Individual patient results are differentiated by color and the cross corresponds to the median value at each time point. Labels indicate patient RECIST v.1.1 BOR. **c**, Exemplary multiplex-IF images from two patients (pt. I (breast cancer, skin) and pt. G (mesothelioma, abdomen)) capture distribution and frequency of B cell foci in the BL and OT paired biopsy tissues. Tumor area annotated in red. Light blue circles, B cells distributed in foci; green, CD20; blue, DAPI (nuclei). **d**, Exemplary multiplex-IF images from patient G. Total view on biopsy sample and enlarged view on individual foci, displaying the increased DC-LAMP$^+$ DC and B cell abundance as well as the colocalization of both cell types on treatment. Tumor area annotated in red. Green, CD20; purple, DC-LAMP; blue, DAPI (nuclei).

https://doi.org/10.1038/s43018-026-01157-8

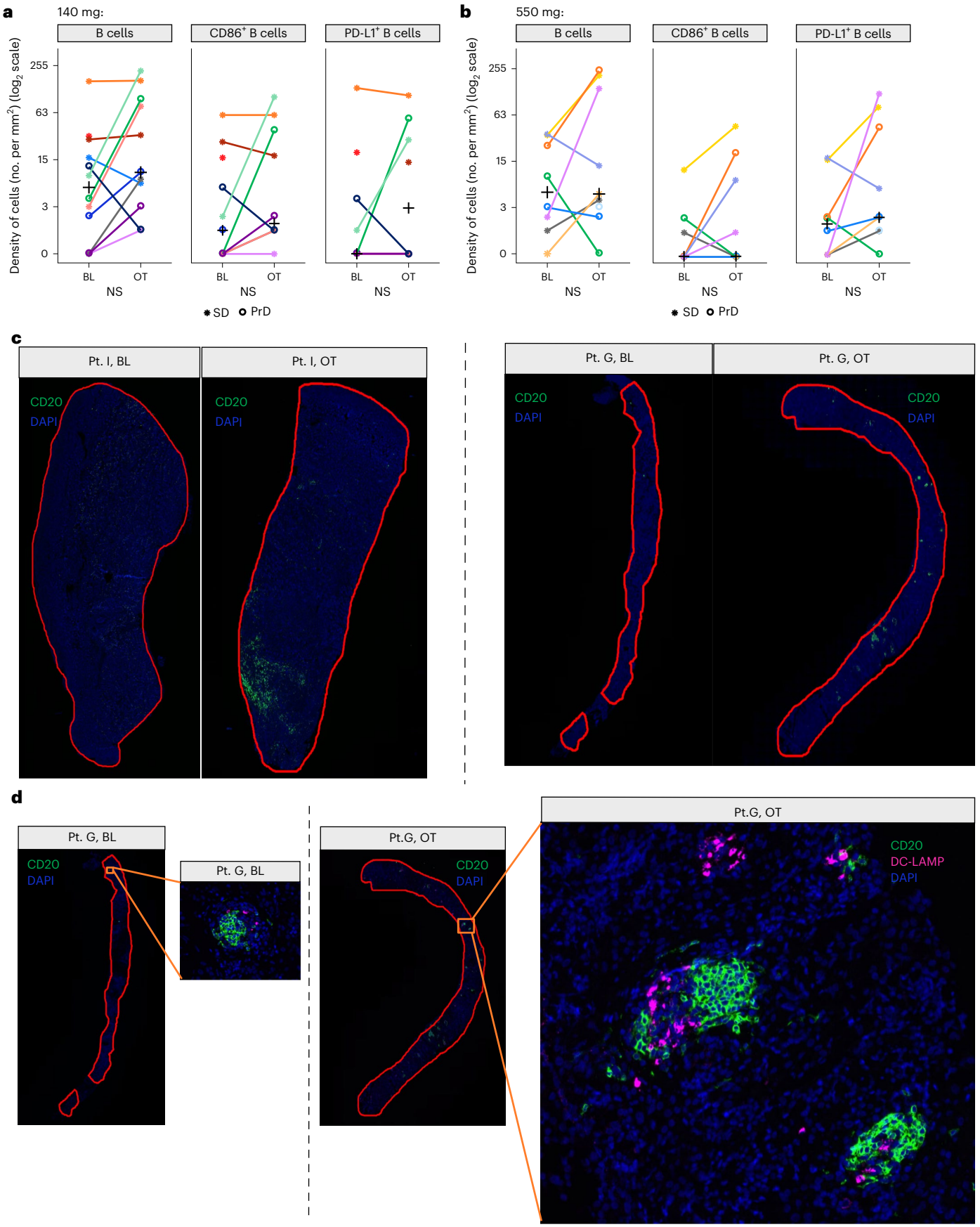

It is unclear whether T cells colocalized within the pre-TLS structures. T cell markers investigated were limited to CD8 and Foxp3 and were not included in the multiplex staining with DC and B cell markers. It also cannot be excluded that the intratumoral PD-L1$^+$ B cells induced by RO7300490 display a regulatory phenotype, as has been shown in glioma after administration of systemic anti-CD40 (ref. 52), along with induced TLS structures.

Hierarchical clustering of gene expression changes after RO7300490 treatment separated the patients into two groups. Cluster II, displaying a gene expression profile associated with lack of immune cell-mediated tumor rejection, was significantly more likely to contain patients with NSCLC, all of which were CPI-experienced. In cluster I, displaying a gene expression profile associated with immune cell activation, there was a trend for enrichment of CPI-naive patients and patients experiencing long SD (≥12 weeks). Although this analysis is limited by low patient numbers and a heterogenous patient population, the results suggest that certain patient subsets may benefit from CD40 pathway activation. Considering that the RO7300490 MOA targets and activates APCs, it is tempting to speculate that combined treatment with an antigen releasing agent to optimize local APC access to tumor antigens (for example low dose radiation therapy or chemotherapy) and a CPI to further enhance T cell activation may be a promising option[58], especially in a CPI-naive population, which limits our ability to fully assess the clinical activity of the molecule.

Study limitations include the small sample size, nonrandomized design and heterogeneous patient population across multiple tumor indications.

In conclusion, the clinical therapeutic window for CD40 agonism can be safely increased to biologically active doses, in line with the expectations for this next-generation targeted CD40 agonist agent. Targeting CD40 agonism to the tumor achieves a strong and sustained target engagement and tumor tissue immunomodulation. These findings warrant further studies in combination with other anticancer agents in earlier therapy lines.

Methods

Study design and patient population

This was an open-label, nonrandomized, multicenter, first-in-human, phase I study. The main study (NCT04857138) and the imaging substudy (at a single site in Spain) complied with all relevant regulations regarding human study participants, were conducted in accordance with the Declaration of Helsinki and were approved by local institutional review boards (IRBs) and/or ethics committees (ECs) (CEIC de Navarra, EC_2021/2; HRA & HCRW, 21/FT/0031; De VK Region Hovedstaden, H-21017757; SNUH IRB, H-2104-078-1211; ASM IRB S2021-0747-0001; and CPP Ile de France I, CPPIDF1-2022-DI21-cat.1), with the substudy approved as an amendment (CEIC de Navarra, EC_2021/2). Participants provided written informed consent and were not compensated. Specimen collection and evaluation were in accordance with informed consent. A redacted protocol is included in Supplementary Information.

Intravenous RO7300490 was administered on day 1 of every 2-week cycle for 24 months or until PrD, unacceptable toxicity, or consent withdrawal. Dose escalation was guided by the modified continual reassessment method (CRM) with escalation with overdose control design[59]. The MTD was defined as the dose with the highest probability of the DLT rate being within a target interval of 20–35%, with a low probability (<25%) of the DLT rate exceeding 35%. A two-parameter logistic model was used to fit the dose–toxicity relationship, and a minimally informative bivariate normal prior was used for the parameters of the DLT dose–response curve. Six ascending dose cohorts involving ≥3 patients were assessed (16 mg, $n = 6$; 48 mg, $n = 4$; 140 mg, $n = 4$; 280 mg, $n = 7$; 550 mg, $n = 4$; and 1,100 mg, $n = 4$). DLTs were monitored from the first dose until 7 days after the second dose. The decision to dose escalate was made by the sponsor and investigators following review of all available data, including safety and PK, and was guided by the CRM. No statistical methods were used to predetermine sample sizes, with enrollment into the dose-escalation cohorts determined by the operating characteristics of the CRM model, as in similar phase I dose-escalation trials.

Additional patients were enrolled into two backfill cohorts (140 mg, $n = 19$ and 550 mg, $n = 24$) to collect paired baseline and on-treatment (day 3 of cycle 3) biopsies for PD analysis. Sample sizes were determined empirically, with the aim being to collect approximately ten evaluable paired biopsies, sufficient to detect a difference of one s.d. This target was selected based on previous CD8 PD analyses in immunotherapy trials,[60] accounting for anticipated biopsy failure rates.

In the one-cycle, nonrandomized, open-labeled, imaging substudy, PET/computed tomography (CT) was used with [^{89}Zr]Zr-RO7300490 to determine RO7300490 tissue biodistribution. [^{89}Zr]Zr-RO7300490 was manufactured at VU University Medical Center Amsterdam. Patients were enrolled into two imaging cohorts, at labeled doses of 140 or 550 mg, after the safety and tolerability of each dose was confirmed. Patients received a single intravenous dose of 135 or 545 mg unlabeled RO7300490, followed by 5 mg [^{89}Zr]Zr-RO7300490. Clinical grade RO7300490 was coupled with the bifunctional chelator DFO-Bz-NCS (Macrocyclics) and labeled with ^{89}Zr (BV Cyclotron VU) according to good manufacturing practice standards with validated production processes and release criteria[61]. [^{89}Zr]Zr-RO7300490 was administered ~40 h after its release. RO7300490 was continued from cycle 2 onwards in the main study. Patients in the substudy did not undergo biopsy.

Patients aged ≥18 years with advanced and/or metastatic solid tumors that had progressed on previous cancer therapy or were not amenable to standard therapy, including NSCLC, small cell lung cancer, triple negative breast cancer, cutaneous melanoma, urothelial cancer, mesothelioma, hepatocellular carcinoma, head and neck squamous cell carcinoma, esophageal squamous cell carcinoma and cervical squamous cell carcinoma, were enrolled. A wash-out period of 28 days or five half-lives of previous drug(s), whichever was shorter, was required before the first RO7300490 administration. Patients had an Eastern Cooperative Oncology Group performance status of 0 or 1, adequate bone marrow, renal, hepatic, coagulation and cardiovascular functions (Supplementary Table 2), and measurable disease per RECIST v.1.1 criteria. Patients enrolled into the backfill cohorts had lesions that could be safely biopsied. Patients with untreated brain metastases, autoimmune disorders, coagulopathies or notable comorbidities were excluded.

Safety

The primary end points (incidence, nature and severity of AEs), were summarized per dose level. AEs were mapped using MedDRA v.26.1 and graded according to National Cancer Institute Common Terminology Criteria for Adverse Events v.5.0, except for CRS, which was graded using American Society for Transplantation and Cellular Therapy criteria[62]. AEs considered DLTs are presented in Supplementary Table 3. Patients who received ≥1 RO7300490 dose were safety evaluable.

Efficacy

The secondary end points relating to efficacy (objective response rate, DCR, duration of response and PFS), were summarized per dose level. Tumor assessments were performed at screening, weeks 6, 12, 18 and every 12 weeks thereafter, using a CT scan with contrast (or magnetic resonance imaging). Responses were categorized according to RECIST v.1.1 by the investigator. Patients who received ≥1 RO7300490 dose and had ≥1 post-baseline tumor assessment after 6 weeks or discontinued the study due to symptomatic deterioration before the first on-study tumor assessment were efficacy evaluable. Patients with missing or no response assessments were classified as not evaluable unless there was documented clinical deterioration, in which case the patient was classified as a nonresponder. Time-to-event end points were censored at the day of the last tumor assessment for patients without documented PrD

or death. Exploratory subgroup analyses were performed based on CPI status or number of previous lines of anticancer therapy. Prolonged SD was defined as disease remaining stable per RECIST v.1.1 for ≥12 weeks (84 days) since the start of study treatment.

[^{89}Zr]Zr-RO7300490 tumor uptake

The primary end points of the imaging substudy utilized standardized uptake value (SUV) metrics to quantify [^{89}Zr]Zr-RO7300490 uptake in tumor lesions and healthy organs. Imaging assessments included a baseline [^{18}F]-FDG-PET/CT (FDG-PET) scan and up to four [^{89}Zr]Zr-RO7300490 PET/CT (^{89}Zr-PET) scans on treatment (2 (day 1), 24 (day 2), 96 (day 5) and 168 h (day 8) post-infusion). Analysis was performed by a nuclear medicine physician experienced in PET/CT imaging. To quantify specific tumor uptake under different mass doses, TBR based on maximum SUV was used, which also considers the uptake signal in blood (descending aorta as reference region). Tumor lesions with positive signal on FDG-PET were segmented using semi-automated and manual methods. Relative threshold cutoffs of maximum uptake values within any given lesion region were used as starting point. Manual edits were made to adjust volume of interest (VOI) boundaries to account for missed regions of elevated uptake or to remove regions of high signal from adjacent organs. Lesion VOIs delineated on FDG-PET scans were transferred to ^{89}Zr-PET scans. If a lesion was identified on FDG-PET but no uptake was detected on ^{89}Zr-PET, the VOI were transferred onto the ^{89}Zr-PET using anatomical landmarks only. Up to ten lesions per patient were delineated. All patients consented to the publication of medical images using their individual participant ID.

Pharmacokinetics

Characterizing the PK parameters (clearance (CL) and volume of distribution (V) at steady state) of RO7300490 was a secondary study end point. Serum RO7300490 was quantified using a one-step electrochemiluminescence immunoassay on the Cobas e411 immunoanalyzer platform. Biotinylated rH-Cd40 receptor (rH-CD40-Bi, mono) was used as capture molecule, with Ru(bpy) human FAP (huFAP-SRu (NHS)) as a detection molecule, and streptavidin-coated complexes were visualized with the chemiluminescent co-reactant tripropylamine. Calibrators (RO7300490) and quality control samples were analyzed in parallel to the test samples using a bioanalytical validated assay. The PK-evaluable population included 80 patients who received ≥1 dose of RO7300490 and had ≥1 PK post-dose sample. Overall, 1,742 of 1,931 analyzed PK samples were evaluable and 189 (9.79%) were below the lower limit of quantification (1.16 ng ml^{-1}). RO7300490 PK showed a TMDD, which could be well described by a TMDD population PK model using the quasi-steady-state approximation as described by Gibiansky and Gibiansky[63]; evaluation and simulation were carried out with NONMEM software v.7.5.1. Graphical analyses were performed with R v.4.3.1 using R studio (2023).

Immunogenicity

ADA incidence to RO7300490 was a secondary end point. ADA measurements were conducted on the Cobas e411 immunoanalyzer platform. Before analysis, test samples, negative controls and ADA-positive controls were incubated with a suppressor-reagent that binds to soluble (s) FAP in the sample matrix (serum) and blocks sFAP from binding to the labeled capture (RO7300490-Bi) and detection (RO7300490-Ru) molecules. The chemiluminescent agent was tripropylamine. The ADA-evaluable population included 75 of a total of 80 patients who received at least one RO7300490 dose and had at least one post-baseline ADA sample.

Flow cytometry

The RO of CD40 by RO7300490 was determined using a flow cytometry-based assay (see list of antibodies in Supplementary Table 4). Whole blood collected in sodium heparin was prepared following standard protocols. RO was determined using the bound receptor approach with the use of an ADA specific for the PG_LALA mutation on RO7300490. The following three conditions were measured: mean fluorescent intensity (MFI) of effectively bound RO7300490 (MFI effective binding); MFI of negative control binding corresponding to background fluorescence (MFI neg control binding); and MFI of saturated RO7300490 binding (MFI saturation binding). The percentage of RO was calculated by RO (% = 100 × ((MFI effective binding − MFI neg control binding)/(MFI saturation binding − MFI neg control binding)).

Blood samples for immunophenotyping were collected in Cyto-Chex Blood Collection Tubes (Streck) and sent at ambient temperature for sample preparation and flow cytometry analysis according to validated assay protocols. Cell preparation was carried out according to manufacturer's instructions (https://www.bdbiosciences.com/en-ch/products/reagents/flow-cytometry-reagents/clinical-diagnostics/multitest-6-color-tbnk-kit). A list of antibodies is in Supplementary Table 5.

Immune cell subsets (T, B, natural killer (NK) cells and monocytes) and RO were analyzed using a standard hierarchical gating strategy on CD45^{+} singlets and lineage markers, comparable to fit-for-purpose validated methods previously described[64]. Data acquisition for the CD40 RO assay was conducted using FACS Canto II (ten-color, three-laser) instruments (BD Biosciences). Data acquisition for the phenotyping assay was conducted using FACS Canto II (eight-color, three-laser) instruments (BD Biosciences). Analysis of CD40 RO and T, B, and NK cell assays was conducted using FACSDiva acquisition templates tailored to each specific assay (BD Biosciences). Data analysis was performed with FACSDiva software (BD Biosciences).

Cytokines

Peripheral cytokine levels were measured by ELISA utilizing the Protein Simple ELLA Cartridge SPCKC-PS-001845 (CD25/sIL-2R, IL-6, IL-8, IP-10/CXCL10).

PD effects in tumor tissue

The PD effects of RO7300490 were investigated in two backfill cohorts at 140 and 550 mg. These doses were selected based on the expected exposure of RO7300490 in the tumor tissue, considering CD40 RO results, population PK dose modeling, and tumor imaging data, and allowed testing at exposures that achieved either transient or persistent saturation of CD40. Tumor biopsies were collected pretreatment and 48 h after the third cycle, preferentially from the same location. All samples were processed and paraffin-embedded according to standardized histopathology protocols. Formalin-fixed paraffin-embedded (FFPE) blocks were sectioned consecutively at 3 µm (IF assay) or 4 µm (hematoxylin and eosin stain and IHC assays). Only samples passing quality control for sufficient tumor content without necrotic areas and excluding major lymph node tissue contamination were included. Due to the scarcity and high variability of the cells of interest, particularly DCs, data were analyzed by individual dose cohorts and by pooling both cohorts. Details on the analyzed biopsy samples can be found in Supplementary Table 6.

FAP and CD8/FoxP3/GZMB-triplex IHC

The Ventana FAP (SP325) assay (Ventana Medical Systems) was used according to manufacturer's instructions. A FAP staining protocol (list of antibodies in Supplementary Table 7) developed and validated with the OptiView detection kit was used to stain FFPE sections on a Benchmark ULTRA staining platform. Slides were visually scored by a board-certified pathologist. FAP was reported as the percentage of FAP-positive cells in the tumor area (epithelium and stroma).

A chromogenic CD8/FoxP3/GZMB-triplex assay protocol was applied on FFPE sections using a Ventana Discovery ULTRA platform (see list of antibodies in Supplementary Table 7). Whole slide images were digitized with a ×20 objective deploying Panoramic scan devices

(3DHistech). Upon annotation of the tumor area, CD8/FOxP3/GZMB cells were quantified by a validated automatic image analysis scoring algorithm using Visiopharm software and quality checked by a pathologist.

LAMP3/CLEC9a/CLEC10a/CD20/CD70/CD68$^+$163/CD86/CD279-multiplex-IF

A validated custom developed eight-plex IF panel (in situplex) was performed applying Ultivue technology. The markers used were optimized for specific identification of DC-LAMP$^+$ mature DCs, CLEC9A$^+$ cDC1 and CLEC10A$^+$ classical type2 DCs (cDC2), macrophages (CD68/CD163) and B cells (CD20; see list of antibodies in Supplementary Table 8). This selection was informed by the analysis of CD40 expression in single-cell RNA sequencing datasets on tumor-infiltrating lymphocytes[65].

FFPE sections were stained on the BOND RX staining platform. Whole slide images were digitized at ×20 magnification. Round 1 and 2 images were co-registered and stacked with Ultivue's UltiStacker software. Upon annotation, defined cell types were quantified by a validated automatic image analysis scoring algorithm using Visiopharm software and quality checked by a pathologist. CD70 results were noninformative and are not presented.

Immunofluorescence data analysis

For each cell type and feature, samples were excluded if only one time point (either baseline or on treatment) was available. As the data do not follow a normal distribution and show some extreme values that could not be classified as outliers due to lack of abnormalities in the IF images, the Wilcoxon signed-rank test (two-sided) was used to determine the statistical significance of baseline versus on-treatment comparisons. Due to the high variability inherent to IHC data and the different potential biological considerations for multiple testing corrections, raw *P* values are reported. Corrected *P* values were also computed using the FDR method, after checking for potential high correlations (correlation coefficient ≥0.8) between the five different cell types. For example, for the density of CD86$^+$ cells, a correlation of 0.94 between cDC2 and macrophage cells resulted in 5 − 1 = 4 tests for FDR correction.

Gene expression profiling and data analysis

Total RNA was isolated from macro-dissected FFPE tumor tissue sections using the QIAGEN AllPrep DNA/RNA FFPE kit according to manufacturer's instructions. RNA was subjected to library preparation with the Illumina TruSeq RNA Exome kit, which is a hybridization-based assay to enrich coding RNAs from total RNA sequencing libraries. RNA libraries were sequenced on a NovaSeq 6000 instrument (Illumina) at a targeted read depth of 25 M per sample. Base calling (BCL) was performed with BCL to FASTQ file converter bcl2fastq2 v.2.20.0 (Illumina). FASTQ files were quality checked with FastQC v.0.11.9 (ref. 66). Reads were mapped to the human genome using STAR v.2.7.3a and default parameters[67]. Aligned reads were quality checked with MultiQC 1.9 (ref. 68). Numbers of mapped reads were combined into a single value (count) per gene using featureCounts v.2.0.1 (ref. 69) assuming a reverse-stranded library and normalized as transcripts per million. All samples passed quality control and were retained, except three samples that did not pass histology criteria (due to cytology-like morphology on baseline or residual lymph node tissue). Genes expressed at >1 counts per million (cpm) in ≥8 samples were further processed in R v.4.2.0 (ref. 70) and the packages limma v.3.54.2 (ref. 71) and edgeR v.3.40.2 (ref. 72). Differential gene expression analysis was performed using all paired samples and genes expressed at cpm >1 in ≥4 samples, by applying voom-limma and the model ~ 0 + patient + Visit[73]. Estimated $\log_2$ fold changes ($\log_2$FC) on-treatment versus baseline across patients and FDR-corrected *P* values were reported. Signature enrichment analysis was performed using CAMERA[74]. FDR-corrected *P* values and median $\log_2$FC across all genes of a signature were reported. Employed signatures were based on previous publications[75–78] (Supplementary Table 9).

To identify distinct groups of patients, we performed hierarchical clustering of on-treatment versus baseline signature $\log_2$FC values per individual as implemented in ComplexHeatmap in R, using default parameters (distance = 'euclidean', method = 'complete') and displaying all values as a heatmap. The resulting dendrogram was cut at the first level, dividing patients into two distinct groups based on their similarity of treatment-induced changes. To assess the association between the two patient clusters (Hclust) and patient metadata (variables IndicationSimple (simplified indication), Long SD (RECIST 1.1 BOR of SD with a minimum duration of ≥12 weeks), FAP_IHC (FAP levels assessed by IHC), ACTARM (backfill cohort arm) and CPI (CPI treatment history)), we performed logistic regression analysis using the glm function (stats package, R), family = 'binomial', and reported results as odds ratios and *P* values.

Statistical analyses

The primary objective was to evaluate the safety and tolerability of RO7300490 and identify the MTD. Secondary objectives included evaluation of efficacy, PK and immunogenicity. Exploratory objectives focused on the drug's MOA. The imaging substudy objective was to evaluate drug tumor uptake.

For safety, efficacy and PK analyses, data were pooled based on the patient's assigned dose level (the effective dose level received on cycle 1 day 1 for safety and efficacy and the actual dose level received for PK analysis), irrespective of the cohort in which the patient was enrolled or intra-patient dose escalation. For the analyses of peripheral PD, data from the dose-escalation and backfill cohorts were pooled based on the patient's assigned dose level. Descriptive statistics were used to summarize baseline characteristics, exposure and disposition, clinical efficacy and safety. Kaplan–Meier methodology was used to estimate median time-to-event endpoints with associated 95% CI. Descriptive statistics were used to summarize PK data and derived RO from the TMDD population PK model. Two-tailed *t*-test and Mann–Whitney tests were used to analyze the differences in tumor uptake between the imaging dose groups. For detailed description of the methods performed to analyze PD data (RNA sequencing and IF data), see the respective sections on IF data analysis and gene expression profiling. A value of $P < 0.05$ was considered statistically significant.

Data collection and analysis were performed without blinding. Data distributions were assumed to be normal, but this was not formally tested. $\log_2$ transformation was applied where needed to approximate normality, and nonparametric methods were used otherwise.

Reporting summary

Further information on research design is available in the Nature Portfolio Reporting Summary linked to this article.

Data availability

For eligible studies, qualified researchers may request access to individual patient level clinical data through a data request platform. At the time of writing, this request platform is Vivli (https://vivli.org/ourmember/roche/). For up-to-date information on Roche's Global Policy on the Sharing of Clinical Information and how to request access to related clinical study documents, see here: https://go.roche.com/data_sharing. Source data for all figures and extended data figures have been provided as source data files. All other data supporting the findings of this study, along with model specifications, files and qualification, including final modeling parameters, are available from the corresponding author on reasonable request. RNA sequencing data cannot be made available due to regional secondary data use restrictions, data privacy and participant re-identification risks. Medical imaging data (DICOM images) are considered sensitive personal health information and there is currently no safe environment for sharing this kind of data. Anonymized records for individual patients across more than one data source external to Roche cannot, and should not,

be linked due to a potential increase in risk of patient re-identification. Source data are provided with this paper.

References

1. Elgueta, R. et al. Molecular mechanism and function of CD40/CD40L engagement in the immune system. *Immunol. Rev.* **229**, 152–172 (2009).
2. French, R. R., Chan, H. T., Tutt, A. L. & Glennie, M. J. CD40 antibody evokes a cytotoxic T-cell response that eradicates lymphoma and bypasses T-cell help. *Nat. Med.* **5**, 548–553 (1999).
3. Vonderheide, R. H. CD40 agonist antibodies in cancer immunotherapy. *Annu. Rev. Med.* **71**, 47–58 (2020).
4. Vonderheide, R. H. et al. Clinical activity and immune modulation in cancer patients treated with CP-870,893, a novel CD40 agonist monoclonal antibody. *J. Clin. Oncol.* **25**, 876–883 (2007).
5. Rüter, J., Antonia, S. J., Burris, H. A., Huhn, R. D. & Vonderheide, R. H. Immune modulation with weekly dosing of an agonist CD40 antibody in a phase I study of patients with advanced solid tumors. *Cancer Biol. Ther.* **10**, 983–993 (2010).
6. Furman, R. R., Forero-Torres, A., Shustov, A. & Drachman, J. G. A phase I study of dacetuzumab (SGN-40, a humanized anti-CD40 monoclonal antibody) in patients with chronic lymphocytic leukemia. *Leuk. Lymphoma* **51**, 228–235 (2010).
7. Johnson, P. et al. Clinical and biological effects of an agonist anti-CD40 antibody: a Cancer Research UK phase I study. *Clin. Cancer Res.* **21**, 1321–1328 (2015).
8. Moreno, V. et al. A phase 1 study of intravenous mitazalimab, a CD40 agonistic monoclonal antibody, in patients with advanced solid tumors. *Invest. New Drugs* **41**, 93–104 (2023).
9. Coveler, A. L. et al. Phase 1 dose-escalation study of SEA-CD40: a non-fucosylated CD40 agonist, in advanced solid tumors and lymphomas. *J. Immunother. Cancer* https://doi.org/10.1136/jitc-2022-005584 (2023).
10. Bajor, D. L. et al. Long-term outcomes of a phase I study of agonist CD40 antibody and CTLA-4 blockade in patients with metastatic melanoma. *Oncoimmunology* **7**, e1468956 (2018).
11. Tran, B. et al. A phase 1 study of the CD40 agonist MEDI5083 in combination with durvalumab in patients with advanced solid tumors. *Immunotherapy* **16**, 759–774 (2024).
12. Vonderheide, R. H. et al. Phase I study of the CD40 agonist antibody CP-870,893 combined with carboplatin and paclitaxel in patients with advanced solid tumors. *Oncoimmunology* **2**, e23033 (2013).
13. Dziadek, S. et al. Comprehensive analysis of fibroblast activation protein expression across 23 tumor indications: insights for biomarker development in cancer immunotherapies *Front. Immunol*. https://doi.org/10.3389/fimmu.2024.1352615 (2024).
14. Scanlan, M. J. et al. Molecular cloning of fibroblast activation protein a, a member of the serine protease family selectively expressed in stromal fibroblasts of epithelial cancers. *Proc. Natl Acad. Sci. USA* **91**, 5657–5661 (1994).
15. Melero, I. et al. A first-in-human study of the fibroblast activation protein–targeted, 4-1BB agonist RO7122290 in patients with advanced solid tumors. *Sci. Transl. Med.* **15**, eabp9229 (2023).
16. Steeghs, N. et al. Safety, pharmacokinetics, pharmacodynamics, and antitumor activity from a phase I study of simlukafusp alfa (FAP-IL2v) in advanced/metastatic solid tumors. *Clin. Cancer Res.* **30**, 2693–2701 (2024).
17. Chen, L. et al. FAP positive fibroblasts induce immune checkpoint blockade resistance in colorectal cancer via promoting immunosuppression. *Biochem. Biophys. Res. Comm.* **487**, 8–14 (2017).
18. Herrera, M. et al. Prognostic interactions between FAP^+ fibroblasts and $CD8a^+$ T cells in colon cancer. *Cancers* **12**, 3238 (2020).
19. Sum, E. et al. Fibroblast activation protein α-targeted CD40 agonism abrogates systemic toxicity and enables administration of high doses to induce effective antitumor immunity. *Clin. Cancer Res.* **27**, 4036–4053 (2021).
20. Brennen, W. N., Isaacs, J. T. & Denmeade, S. R. Rationale behind targeting fibroblast activation protein-expressing carcinoma-associated fibroblasts as a novel chemotherapeutic strategy. *Mol. Cancer Ther.* **11**, 257–266 (2012).
21. Kooten, C. V. & Banchereau, J. Functions of CD40 on B cells, dendritic cells and other cells. *Curr. Opin. Immunol.* **9**, 330–337 (1997).
22. Böttcher, J. P. & Reis e Sousa, C. The role of type 1 conventional dendritic cells in cancer immunity. *Trends Cancer* **4**, 784–792 (2018).
23. den Haan, J. M. M., Lehar, S. M. & Bevan, M. J. $CD8^+$ but not $CD8^-$ dendritic cells cross-prime cytotoxic T cells in vivo. *J. Exp. Med.* **192**, 1685–1696 (2000).
24. Arruda, L. B. et al. Dendritic cell-lysosomal-associated membrane protein (LAMP) and LAMP-1-HIV-1 gag chimeras have distinct cellular trafficking pathways and prime T and B cell responses to a diverse repertoire of epitopes. *J. Immunol.* **177**, 2265–2275 (2006).
25. de Saint-Vis, B. et al. A novel lysosome-associated membrane glycoprotein, DC-LAMP, induced upon DC maturation, is transiently expressed in MHC class II compartment. *Immunity.* **9**, 325–336 (1998).
26. Hildner, K. et al. Batf3 deficiency reveals a critical role for $CD8\alpha^+$ dendritic cells in cytotoxic T cell immunity. *Science* **322**, 1097–1100 (2008).
27. Teijeira, A. et al. Depletion of conventional type-1 dendritic cells in established tumors suppresses immunotherapy efficacy. *Cancer Res.* **82**, 4373–4385 (2022).
28. Sánchez-Paulete, A. R. et al. Cancer immunotherapy with immunomodulatory anti-CD137 and anti-PD-1 monoclonal antibodies requires BATF3-dependent dendritic cells. *Cancer Discov.* **6**, 71–79 (2016).
29. Ferris, S. T. et al. cDC1 prime and are licensed by CD4(+) T cells to induce anti-tumour immunity. *Nature* **584**, 624–629 (2020).
30. Ladányi, A. et al. Density of DC-LAMP(+) mature dendritic cells in combination with activated T lymphocytes infiltrating primary cutaneous melanoma is a strong independent prognostic factor. *Cancer Immunol. Immunother.* **56**, 1459–1469 (2007).
31. Spranger, S. et al. Density of immunogenic antigens does not explain the presence or absence of the T-cell-inflamed tumor microenvironment in melanoma. *Proc. Natl Acad. Sci. USA* **113**, E7759–e7768 (2016).
32. Fridman, W. H. et al. Tertiary lymphoid structures and B cells: an intratumoral immunity cycle. *Immunity* **56**, 2254–2269 (2023).
33. Mohr, P. et al. Advances and challenges in immunoPET methodology. *Front. Nucl. Med.* https://doi.org/10.3389/fnume.2024.1360710 (2024).
34. Irenaeus, S. M. M. et al. First-in-human study with intratumoral administration of a CD40 agonistic antibody, ADC-1013, in advanced solid malignancies. *Int. J. Cancer* **145**, 1189–1199 (2019).
35. Luke, J. J. et al. Phase I study of ABBV-428, a mesothelin-CD40 bispecific, in patients with advanced solid tumors. *J. Immunother. Cancer* https://doi.org/10.1136/jitc-2020-002015 (2021).
36. Medina-Echeverz, J. et al. Systemic agonistic anti-CD40 treatment of tumor-bearing mice modulates hepatic myeloid-suppressive cells and causes immune-mediated liver damage. *Cancer Immunol. Res.* **3**, 557–566 (2015).
37. Siwicki, M. et al. Resident Kupffer cells and neutrophils drive liver toxicity in cancer immunotherapy. *Sci. Immunol.* **6**, eabi7083 (2021).
38. Bonnans, C. et al. CD40 agonist-induced IL-12p40 potentiates hepatotoxicity. *J. Immunother. Cancer* **8**, e000624 (2020).

39. Young, L. S. CD40 activation induces apoptosis in cultured human hepatocytes via induction of cell surface fas ligand expression and amplifies fas-mediated hepatocyte death during allograft rejection. *J. Exp. Med.* **189**, 441–446 (1999).
40. Croft, A. P. et al. Distinct fibroblast subsets drive inflammation and damage in arthritis. *Nature* **570**, 246–251 (2019).
41. Fan, A. et al. Inhibition of fibroblast activation protein ameliorates cartilage matrix degradation and osteoarthritis progression. *Bone Res.* **11**, 3 (2023).
42. Brokopp, C. E. et al. Fibroblast activation protein is induced by inflammation and degrades type I collagen in thin-cap fibroatheromata. *Eur. Heart J.* **32**, 2713–2722 (2011).
43. Mohmand-Borkowski, A. et al. Fibroblast activation protein compared with other markers of activated smooth muscle cells, extracellular matrix turnover and inflammation in a mouse model of atherosclerosis. *Metabolites* **15**, 243 (2025).
44. Scott, A. M. et al. A Phase I dose-escalation study of sibrotuzumab in patients with advanced or metastatic fibroblast activation protein-positive cancer. *Clin. Cancer Res.* **9**, 1639–1647 (2003).
45. Hofheinz, R.-D. et al. Stromal antigen targeting by a humanised monoclonal antibody: an early phase II trial of sibrotuzumab in patients with metastatic colorectal cancer. *Onkologie* **26**, 44–48 (2003).
46. Cheng, S. et al. A pan-cancer single-cell transcriptional atlas of tumor infiltrating myeloid cells. *Cell* **184**, 792–809 (2021).
47. Movassagh, M. et al. Selective accumulation of mature DC-Lamp$^+$ dendritic cells in tumor sites is associated with efficient T-cell-mediated antitumor response and control of metastatic dissemination in melanoma. *Cancer Res.* **64**, 2192–2198 (2004).
48. Dieu-Nosjean, M. C. et al. Long-term survival for patients with non-small-cell lung cancer with intratumoral lymphoid structures. *J. Clin. Oncol.* **26**, 4410–4417 (2008).
49. Germain, C. et al. Presence of B cells in tertiary lymphoid structures is associated with a protective immunity in patients with lung cancer. *Am. J. Respir. Crit. Care Med.* **189**, 832–844 (2014).
50. Truxova, I. et al. Mature dendritic cells correlate with favorable immune infiltrate and improved prognosis in ovarian carcinoma patients. *J. Immunother. Cancer* **6**, 139 (2018).
51. Osorio, J. C. et al. Intratumoral Fc-optimized agonistic CD40 antibody induces tumor rejection and systemic antitumor immunity in patients with metastatic cancer. *Res. Sq.* https://doi.org/10.21203/rs.3.rs-4244833/v1 (2024).
52. van Hooren, L. et al. Agonistic CD40 therapy induces tertiary lymphoid structures but impairs responses to checkpoint blockade in glioma. *Nat. Commun.* **12**, 4127 (2021).
53. Osoria, J. C. et al. Fc-optimized CD40 agonistic antibody elicits tertiary lymphoid structure formation and systemic antitumor immunity in metastatic cancer. *Cancer Cell* **25**, S1535–S6108 (2025).
54. Chow, A., Perica, K., Klebanoff, C. A. & Wolchok, J. D. Clinical implications of T cell exhaustion for cancer immunotherapy. *Nat. Rev. Clin. Oncol.* **19**, 775–790 (2022).
55. Zebley, C. C., Zehn, D., Gottschalk, S. & Chi, H. T cell dysfunction and therapeutic intervention in cancer. *Nat. Immunol.* **25**, 1344–1354 (2024).
56. Arizumi, T. et al. Duration of stable disease is associated with overall survival in patients with advanced hepatocellular carcinoma treated with sorafenib. *Dig Dis.* **32**, 705–710 (2014).
57. van Laarhoven, H. W. et al. When hope is all there is left. *Oncologist* **16**, 914–916 (2011).
58. Labiano, S. et al. CD40 agonist targeted to fibroblast activation protein α synergizes with radiotherapy in murine HPV-positive head and neck tumors. *Clin. Cancer Res.* **27**, 4054–4065 (2021).
59. Neuenschwander, B., Branson, M. & Gsponer, T. Critical aspects of the Bayesian approach to phase I cancer trials. *Stat. Med.* **27**, 2420–2439 (2008).
60. Dejardin, D. et al. A composite decision rule of CD8$^+$ T-cell density in tumor biopsies predicts efficacy in early-stage, immunotherapy trials. *Clin. Cancer Res.* **30**, 877–882 (2024).
61. Vosjan, M. J. et al. Conjugation and radiolabeling of monoclonal antibodies with zirconium-89 for PET imaging using the bifunctional chelate p-isothiocyanatobenzyl-desferrioxamine. *Nat. Protoc.* **5**, 739–743 (2010).
62. Lee, D. W. et al. ASTCT consensus grading for cytokine release syndrome and neurologic toxicity associated with immune effector cells. *Biol. Blood Marrow Transplant.* **25**, 625–638 (2019).
63. Gibiansky, L. & Gibiansky, E. Target-mediated drug disposition model: approximations, identifiability of model parameters and applications to the population pharmacokinetic-pharmacodynamic modeling of biologics. *Expert Opin. Drug Metab. Toxicol.* **5**, 803–812 (2009).
64. Junker, F. et al. A human receptor occupancy assay to measure anti-PD-1 binding in patients with prior anti-PD-1. *Cytometry A* **99**, 832–843 (2021).
65. Schlenker, R. et al. Myeloid-T cell interplay and cell state transitions associated with checkpoint inhibitor response in melanoma. *Medicine* **5**, 759–779 (2024).
66. FastQC v.0.11.9 (Babraham Bioinformatics, 2019).
67. Dobin, A. et al. STAR: ultrafast universal RNA-seq aligner. *Bioinformatics* **29**, 15–21 (2013).
68. Ewels, P., Magnusson, M., Lundin, S. & Käller, M. MultiQC: summarize analysis results for multiple tools and samples in a single report. *Bioinformatics* **32**, 3047–3048 (2016).
69. Liao, Y., Smyth, G. K. & Shi, W. featureCounts: an efficient general purpose program for assigning sequence reads to genomic features. *Bioinformatics* **30**, 923–930 (2014).
70. R v.4.2.0 (R Foundation for Statistical Computing, 2022).
71. Ritchie, M. E. et al. limma powers differential expression analyses for RNA-sequencing and microarray studies. *Nucleic Acids Res.* **43**, e47–e47 (2015).
72. Robinson, M. D., McCarthy, D. J. & Smyth, G. K. edgeR: a Bioconductor package for differential expression analysis of digital gene expression data. *Bioinformatics* **26**, 139–140 (2010).
73. Law, C. W., Chen, Y., Shi, W. & Smyth, G. K. voom: Precision weights unlock linear model analysis tools for RNA-seq read counts. *Genome Biol.* **15**, R29 (2014).
74. Wu, D. & Smyth, G. K. Camera: a competitive gene set test accounting for inter-gene correlation. *Nucleic Acids Res.* **40**, e133 (2012).
75. Cabrita, R. et al. Tertiary lymphoid structures improve immunotherapy and survival in melanoma. *Nature* **577**, 561–565 (2020).
76. Danaher, P. et al. Gene expression markers of tumor infiltrating leukocytes. *J. Immunother. Cancer* **5**, 18 (2017).
77. Combes, A. J. et al. Discovering dominant tumor immune archetypes in a pan-cancer census. *Cell* **185**, 184–203 (2022).
78. Wu, T. D. et al. Peripheral T cell expansion predicts tumour infiltration and clinical response. *Nature* **579**, 274 (2020).

Acknowledgements

This study was sponsored by F. Hoffmann-La Roche. Employees of the sponsor were involved in the design and conduct of the study, the collection, management, analysis and interpretation of the data and preparation of the paper. The authors thank the patients, their families and the participating study centers. The authors also thank all current and former RO7300490 team members as well as their supporting functions for their contributions to the study. Editorial support for the development of this paper, under the direction of the authors, was

provided by D. Matlebjane and C. Wright of Ashfield MedComms, an Inizio company, and funded by F. Hoffmann-La Roche.

Author contributions

Conception or design of study: O.C., B.R. and M.H. (substudy). Acquisition of data: N.K., A.T., I.M., V.M., J.L.B., E.C.A., C.E.A., I.S., D.H.L., J.S., F.T., D.-Y.O., A.H. and S.N.S. Analysis of data: B.R., C.R., A.E., M.H., P.C.S., N.R., G.K., N.A.K. and S.B. Interpretation of data: I.M., B.R., C.R., A.E., N.A.K., C.W., M.H., G.K., N.R., P.C.S., S.B., N.K., A.T., D.J.V., V.M., J.L.B., E.C.A., C.E.A., I.S., D.H.L., J.S., F.T., D.-Y.O., A.H., O.C. and S.N.S. Drafting the article or revising it critically: I.M., B.R., C.R., A.E., N.A.K., C.W., M.H., G.K., N.R., P.C.S., S.B., N.K., A.T., D.J.V., V.M., J.L.B., E.C.A., C.E.A., I.S., D.H.L., J.S., F.T., D-Y.O., A.H., O.C. and S.N.S. Accountability for all aspects of the work: I.M., B.R., C.R., A.E., N.A.K., C.W., M.H., G.K., N.R., P.C.S., S.B., N.K., A.T., D.J.V., V.M., J.L.B., E.C.A., C.E.A., I.S., D.H.L., J.S., F.T., D.-Y.O., A.H., O.C. and S.N.S.

Competing interests

The following competing interests are declared. I.M.: Grants from F. Hoffmann-La Roche, AstraZeneca, BMS and Genmab; honoraria from Curon, Pharmamark, Pioneering Medicines, F. Hoffmann-La Roche, AstraZeneca, BMS, Genmab, Pierre Fabre, F-Star, Merus, Alligator Bioscience AB and Bright Peaks. B.R.: Employed at F. Hoffmann-La Roche; stock ownership at F. Hoffmann-La Roche. C.R.: Employed at F. Hoffmann-La Roche; stock ownership at F. Hoffmann-La Roche. A.E.: Employed at Roche Diagnostics Deutschland; stock ownership at F. Hoffmann-La Roche. N.A.K.: Employed at F. Hoffmann-La Roche. C.W.: Employed at Roche (China) Holding; stock ownership at F. Hoffmann-La Roche. M.H.: Employed at F. Hoffmann-La Roche; stock ownership at F. Hoffmann-La Roche. G.K.: Employed at F. Hoffmann-La Roche; stock ownership at F. Hoffmann-La Roche. N.R.: Employed at Roche Diagnostics GmbH Deutschland; stock ownership at F. Hoffmann-La Roche. P.C.S.: Employed at F. Hoffmann-La Roche; stock ownership at F. Hoffmann-La Roche. S.B.: Employed at F. Hoffmann-La Roche; stock ownership at F. Hoffmann-La Roche. N.K.: Employed at F. Hoffmann-La Roche; stock ownership at F. Hoffmann-La Roche. A.T.: Employed at F. Hoffmann-La Roche; stock ownership at F. Hoffmann-La Roche. D.J.V.: Employed at Amsterdam University Medical Center. V.M.: Employed at START; consultancy with AbbVie, F. Hoffmann-La Roche, Bayer, BMS, Janssen, Syneos, Affimed, AstraZeneca, Merck and Ellipses Pharma; principal investigator for AbbVie; institutional funding from AbbVie, Achilles, Adaptimmune, ADC Therapeutics, Ascendis Pharma, AstraZeneca, Bayer, BeiGene, Bicycle Tx, Bioinvent, Biomea Fusion, BioNTech SE, BMS, Boehringer Ingelheim, C4 Therapeutics, Calico Life Sciences LLC, Celgene, Constellation, Crescendo Biologics, Cullinan, Daiichi Sankyo, Debiopharm, Dragonfly, Enliven Therapeutics, Epizyme, Exelixis, FameWave, F-Star Beta Limited, Genentech, Genmab, Gilead, Grey Wolf Therapeutics, GSK, Hexal AG/Sandoz, HiFiBiO, Hookipa Biotech, Hutchmed, IGM Biosciences, ImCheck Therapeutics, Immunocore, Immutep, Incyte, IOmx Therapeutics, Iovance, Italfarmaco, Iteos, Janssen, Light Chain Bioscience, Lilly, Loxo Oncology, Merck, Merus, Miltenyi Biomedicine, Monta Biosciences, MSD, Mythic Therapeutics, Ningbo Newbay, Novartis, Oxford BioTherapeutics, Pfizer, PharmaMar, PMV Pharma, Prelude Therapeutics Inc, Pyxis Oncology, Regeneron, Relay Therapeutics, Repare Therapeutics, Revolution, F. Hoffmann-La Roche, Schrödinger, Scorpion Therapeutics, Seagen, Shattuck, Synthorx, Takeda, Tango Therapeutics, Tesaro, Totus Medicines, Turning Point Therapeutics and Vividion Therapeutics. J.L.B.: Consultancy with Daiichi Sankyo and Novartis. E.C.A.: Honoraria from GSK, Pfizer, Novartis, F. Hoffmann-La Roche, BMS, Gilead, PI Roche, BMS, AstraZeneca, EISAI, Italfarmaco, IO Biotech, Iovance and MSD. I.S.: Institutional research grants from F. Hoffmann-La Roche, AstraZeneca, Bayer, Boehringer Ingelheim, CDR-Life, Genentech, Incyte, MSD, Orion, Pfizer and Puma Biotechnology; honoraria from AstraZeneca; support for travel, accommodation and congress registration from AstraZeneca and Incyte. J.S.: Stock ownership at Epsilogen and co-founder of Avacta; board membership with Apobec, Discovery; reimbursement to their institution (for recruitment to clinical trials) from Achilles, Gilead, GSK, IO Biotech, MSD, F. Hoffmann-La Roche, RS Oncology and Starpharma; reimbursement to their institution for advisory roles from Apobec, Discovery, Avacta, AstraZeneca, BioNTech, BMS and F. Hoffmann-La Roche. F.T.: Speaker/consultancy/advisory with GSK, BMS, T-knife Therapeutics, Immatics, Scenic Biotec, F-Star, Kite, Leucid, CytomX, Grey Wolf and AstraZeneca; research income from GSK and Novartis. D-Y.O.: Research funding from AstraZeneca, Novartis, Array, Eli Lilly, Servier, BeiGene, MSD and Handon; advisory committees with AstraZeneca, Novartis, Genentech/F. Hoffmann-La Roche, Merck Serono, Bayer, Taiho, ASLAN, Halozyme, Zymeworks, BMS/Celgene, BeiGene, Basilea, Turning Point, Yuhan, Arcus Biosciences, IQVIA, MSD, LG Chem, Astellas, AbbVie, J-Pharma, Mirati Therapeutics, Eutilex, Moderna, Idience, Alligator Bioscience AB and Hana Pharm. A.H.: Consulting fees from Amgen, Sanofi, BMS, Basilea, Incyte, Servier, Relay Therapeutics, Taiho and MSD; honoraria from Incyte, Servier and Seagen; meeting attendance support from Pierre Fabre; participation on a data safety monitoring board or advisory Board for Basilea, QED Therapeutics, Taiho, Relay Therapeutics and MSD. O.C.: Employed at F. Hoffmann-La Roche.; stock ownership at F. Hoffmann-La Roche. S.N.S.: Research funding from MSD & Verastem; advisory committees for Duke St Bio, Ellipses, Exscientia, Grey Wolf Therapeutics, Medannex, MSD and F. Hoffmann-La Roche. The other authors declare no competing interests.

Additional information

Extended data is available for this paper at https://doi.org/10.1038/s43018-026-01157-8.

Supplementary information The online version contains supplementary material available at https://doi.org/10.1038/s43018-026-01157-8.

Correspondence and requests for materials should be addressed to Bernhard Reis.

Peer review information *Nature Cancer* thanks Laurence Buisseret, Haitao Pan, Qian Shi and the other, anonymous, reviewer(s) for their contribution to the peer review of this work.

Reprints and permissions information is available at www.nature.com/reprints.

Publisher's note Springer Nature remains neutral with regard to jurisdictional claims in published maps and institutional affiliations.

Ignacio Melero[1,2,19], Bernhard Reis[3,19] ✉, Corinne Rusterholz[3], Alexandra Epp[4], Nicole A. Kratochwil[5], Chun Wu[6], Michael Hettich[3], Georgios Kazantzidis[7], Natascha Rieder[4], Petra C. Schwalie[5], Solveig Badillo[5], Nadine Kumpesa[5], Andreas Thommen[5], Danielle J. Vugts[8], Victor Moreno[9], Julia Lostes Bardaji[10], Eduardo Castanon Alvarez[11], Carlos E. de Andrea[1], Iben Spanggaard[12], Dae Ho Lee[13], James Spicer[14], Fiona Thistlethwaite[15], Do-Youn Oh[16], Antoine Hollebecque[17], Olivera Cirovic[3] & Stefan N. Symeonides[18]

[1]Clinica Universidad de Navarra, CIMA and CIBERONC, Pamplona, Spain. [2]Nuffield Department of Medicine, University of Oxford, Oxford, UK. [3]Pharma Research and Early Development, Early Development Oncology, Roche Innovation Center Basel, Basel, Switzerland. [4]Pharma Research and Early Development, Early Development Oncology, Roche Innovation Center Munich, Penzberg, Germany. [5]Pharma Research and Early Development, Pharmaceutical Sciences, Roche Innovation Center Basel, Basel, Switzerland. [6]Roche (China) Holding, Shanghai, China. [7]Roche Data Science and Statistics, Biostatistics Oncology, Basel, Switzerland. [8]VU University Medical Center Amsterdam, Amsterdam, Netherlands. [9]START Madrid-FJD, Hospital Fundacion Jimenez Diaz, Madrid, Spain. [10]Vall d'Hebron Institut d'Oncologia, Barcelona, Spain. [11]Clinica Universidad de Navarra, Madrid, Spain. [12]Rigshospitalet, Copenhagen, Denmark. [13]University of Ulsan College of Medicine, Asan Medical Center, Seoul, Korea. [14]King's College London, Guy's Hospital, London, UK. [15]The Christie NHS Foundation Trust and University of Manchester, Manchester, UK. [16]Seoul National University Hospital, Seoul, Korea. [17]Gustave Roussy, Villejuif, France. [18]Edinburgh Cancer Centre, NHS Lothian & Edinburgh Experimental Cancer Medicine Centre, University of Edinburgh, Edinburgh, UK. [19]These authors contributed equally: Ignacio Melero, Bernhard Reis. ✉e-mail: bernhard.reis@roche.com

https://doi.org/10.1038/s43018-026-01157-8

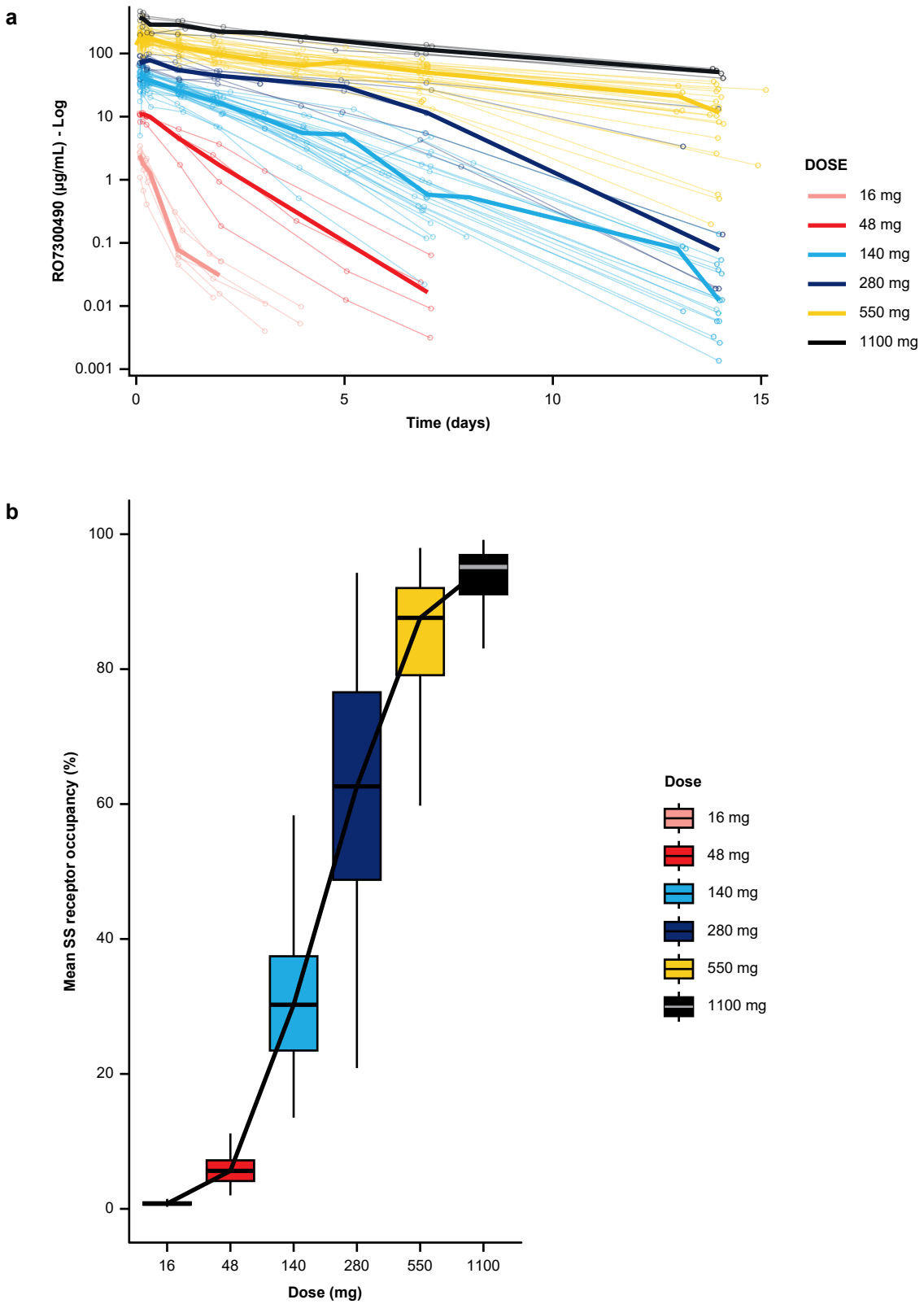

Extended Data Fig. 1 | Pharmacokinetics. a, Median and individual observed serum RO7300490 concentrations over time after the first dose of RO7300490 from evaluable patients who had at least one post-dose PK sample ($n = 80$). Thin lines represent individual profiles, and thick lines represent the median profile per dose level. **b**, Box plot of predicted RO7300490 steady-state TMDD-derived RO for the studied dose range on Q2W schedule, based on the TMDD population PK model (simulation with $n = 1000$ simulated subjects). Boxes represent the median, the 25th, and 75th percentiles (hinges), 1.5 x IQR (interquartile range, lower and upper whiskers). IQR, interquartile range; PK, pharmacokinetics; Q2W, every 2 weeks; RO, receptor occupancy SS, steady-state; TMDD, target-mediated drug disposition.

https://doi.org/10.1038/s43018-026-01157-8

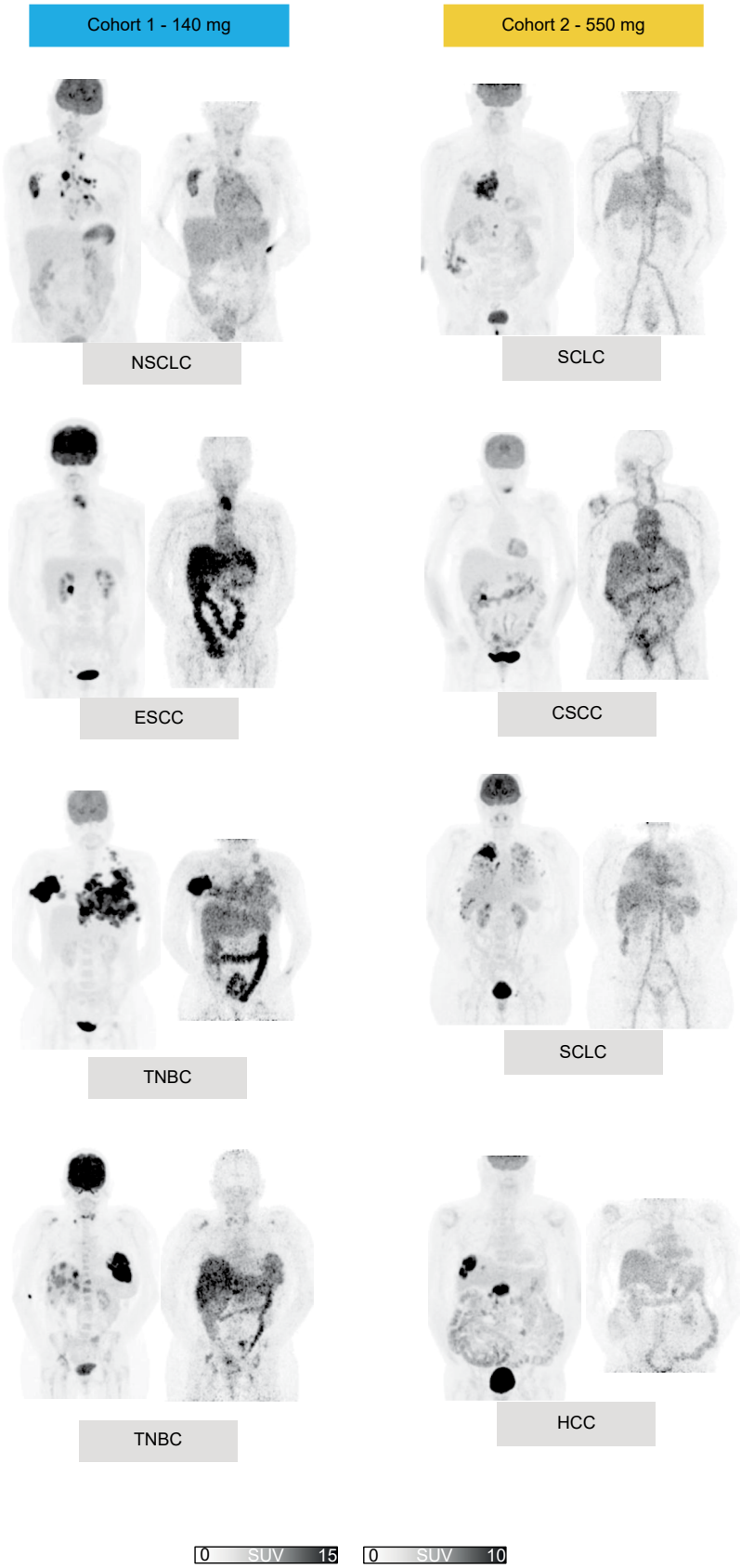

Extended Data Fig. 2 | See next page for caption.

https://doi.org/10.1038/s43018-026-01157-8

Extended Data Fig. 2 | Overview of tumor targeting and in vivo biodistribution of [^{89}Zr]Zr-RO7300490. Representative images of baseline FDG-PET and 96 hours post-dosing [^{89}Zr]Zr-RO7300490 PET scans for all patients of both 140 mg (blue) and 550 mg (yellow). Darker areas indicate high uptake of radiolabeled [^{89}Zr]Zr-RO7300490. Beside tumor tissue, visible uptake beyond background was also observed in non-tumor tissues with known FAP expression, like healing rib cage bone fractures (ESCC) and arthritic joints (CSCC). CSCC, cutaneous squamous cell carcinoma; ESCC, esophageal squamous cell carcinoma; HCC, hepatocellular carcinoma; NSCLC, non-small cell lung cancer; SCLC, small cell lung cancer; TNBC, triple negative breast cancer; SUV, standard uptake value.

https://doi.org/10.1038/s43018-026-01157-8

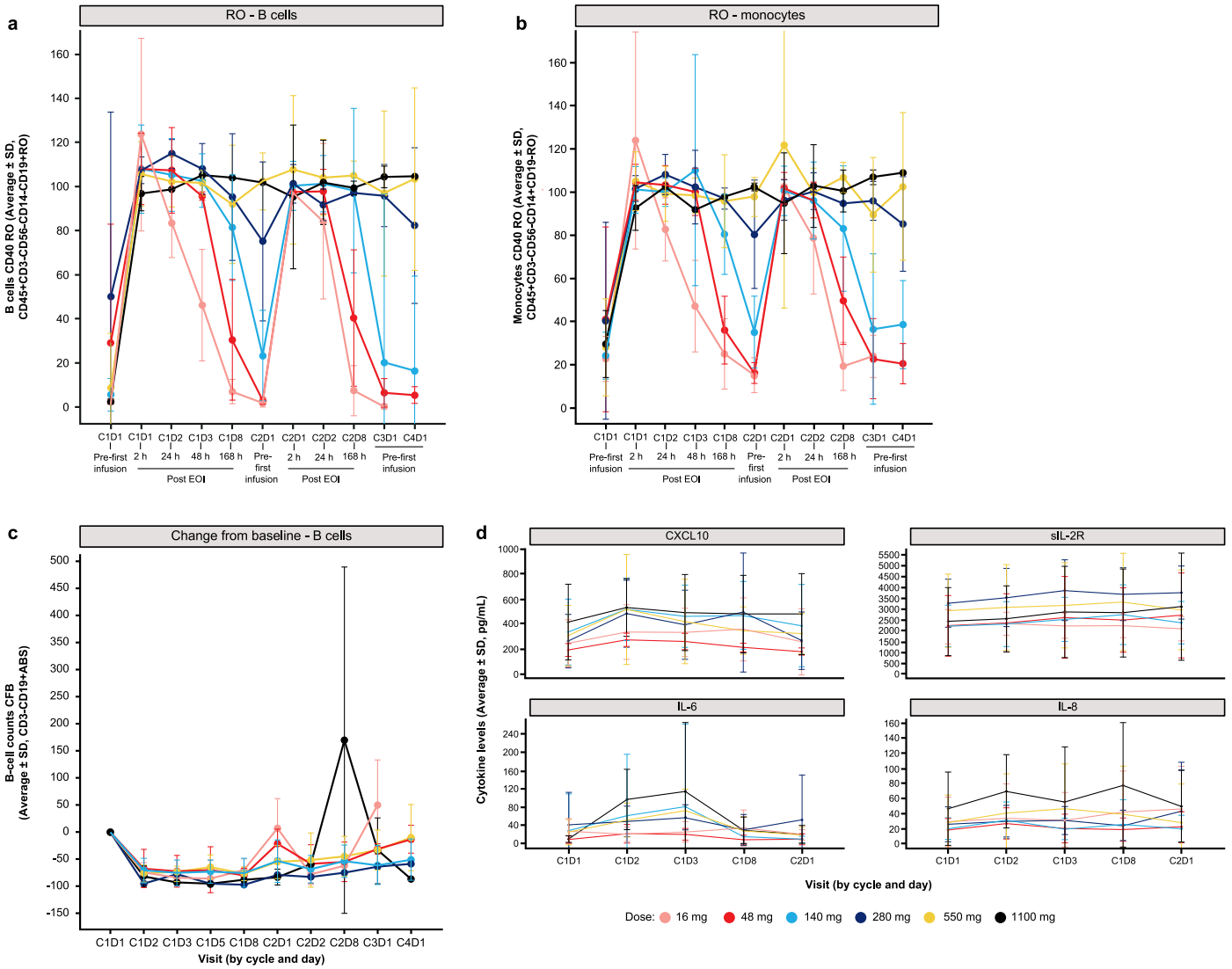

Extended Data Fig. 3 | RO and PD effects in the periphery. Six cohorts were dosed with RO7300490 ranging from 16 up to 1100 mg, see legend for color-coding. Each dosing period is labeled by Cycle ® and the Day (D) at which the sample was collected, for example C1D1 is the first day of the first treatment cycle. All safety-evaluable patients were included in this analysis ($n = 80$). Symbols represent mean measurements of single replicates of patient samples grouped per dose and time point. Error bars represent standard deviations. **a, b**, The percentage of CD40 RO on peripheral blood CD19 + B cells a, and peripheral blood CD14+ monocytes b, determined by flow cytometry is shown. The RO was measured before infusion and at several time points post EOI. **c**, The change from baseline of CD19 + B cell counts (plotted as % change from baseline) was measured using a whole blood flow cytometry-based assay. **d**, Plasma levels in pg/mL of IL-8, sIL-2R, CXCL10 and IL-6 measured by Ella. C, cycle; CFB, change from baseline; D, day; EOI, end of infusion; RO, receptor occupancy.

https://doi.org/10.1038/s43018-026-01157-8

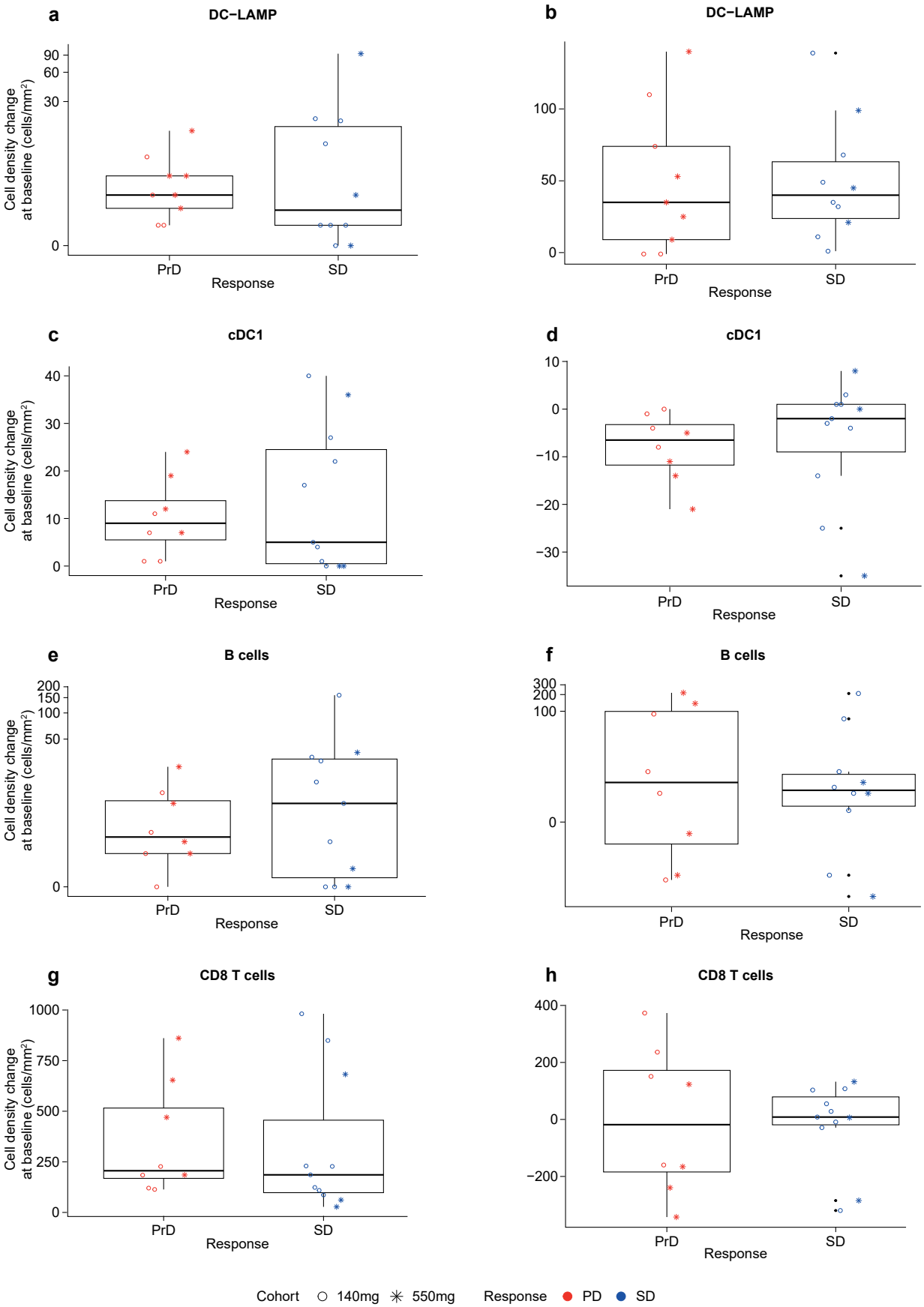

Extended Data Fig. 4 | See next page for caption.

https://doi.org/10.1038/s43018-026-01157-8

Extended Data Fig. 4 | Immune cell subpopulation density analyzed by IF or IHC and their correlation with BOR response. Baseline immune cell densities **a**, **c**, **e**, **g** and immune cell density changes on treatment **b**, **d**, **f**, **h** were plotted according to BOR of SD and PrD. **a, b**, DC-Lamp density and change upon treatment. **c, d**, cDC1 density and change upon treatment. **e, f**, B cell density and change upon treatment. **g, h**, CD8 T-cell density and change upon treatment. For this figure, backfill cohort patients with at least one response assessment were used. Three patients were removed from the analysis as biopsy samples did not pass the quality check, see Table S9 for details (n = 27). The lower and upper hinges of the box plot correspond to the first and third quartiles (the 25th and 75th percentiles). The middle bold line represents the median. The upper whisker extends from the hinge to the largest value no further than 1.5 x IQR (interquartile range) from the hinge. The lower whisker extends from the hinge to the smallest value at most 1.5 x IQR of the hinge. For better visualization, some of the graphs are plotted as log transformed y axis. Density is given as the number of cells/mm^2 tissue.

https://doi.org/10.1038/s43018-026-01157-8

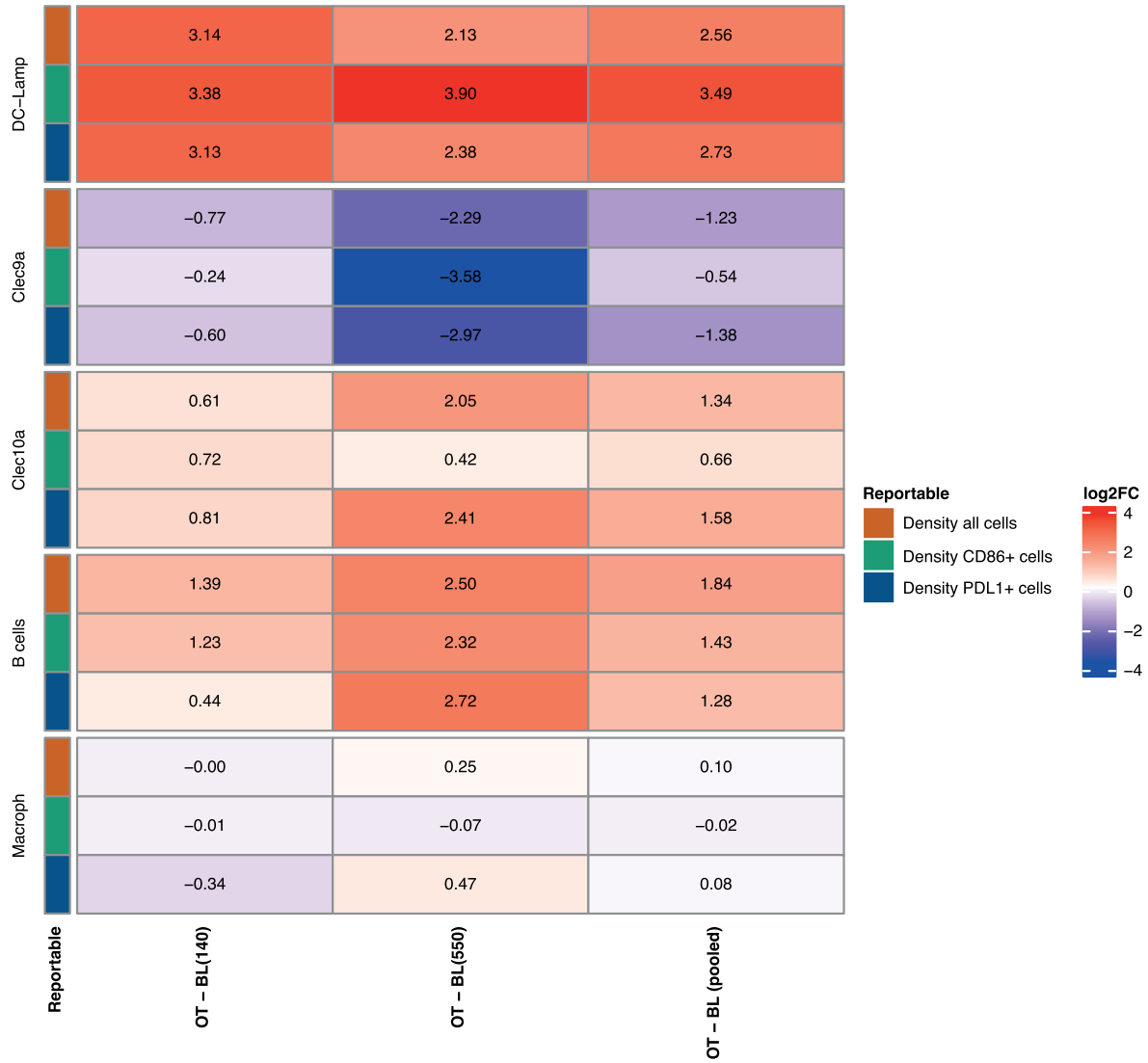

Extended Data Fig. 5 | Summary heatmap visualizing Log2 fold changes (Log2FC) of tissue APC subsets investigated by multiplex-IF in the paired BL and OT biopsies. DC-LAMP: marker for mature DC-LAMP+ DCs, CLEC9A: cDC1; CLEC10A: cDC2; B cells: CD20; macrophages: CD68/CD163. Log2 fold changes from BL to OT samples are shown visually for both cohorts separately and for the pooled data, aggregating both cohorts together. Log2 fold changes of total cells and cells coexpressing CD86 or PD-L1 activation markers are shown, respectively. BL, baseline; DC-LAMP + DC, DC-lysosomal associated membrane protein-positive dendritic cell; OT, on-treatment.

https://doi.org/10.1038/s43018-026-01157-8

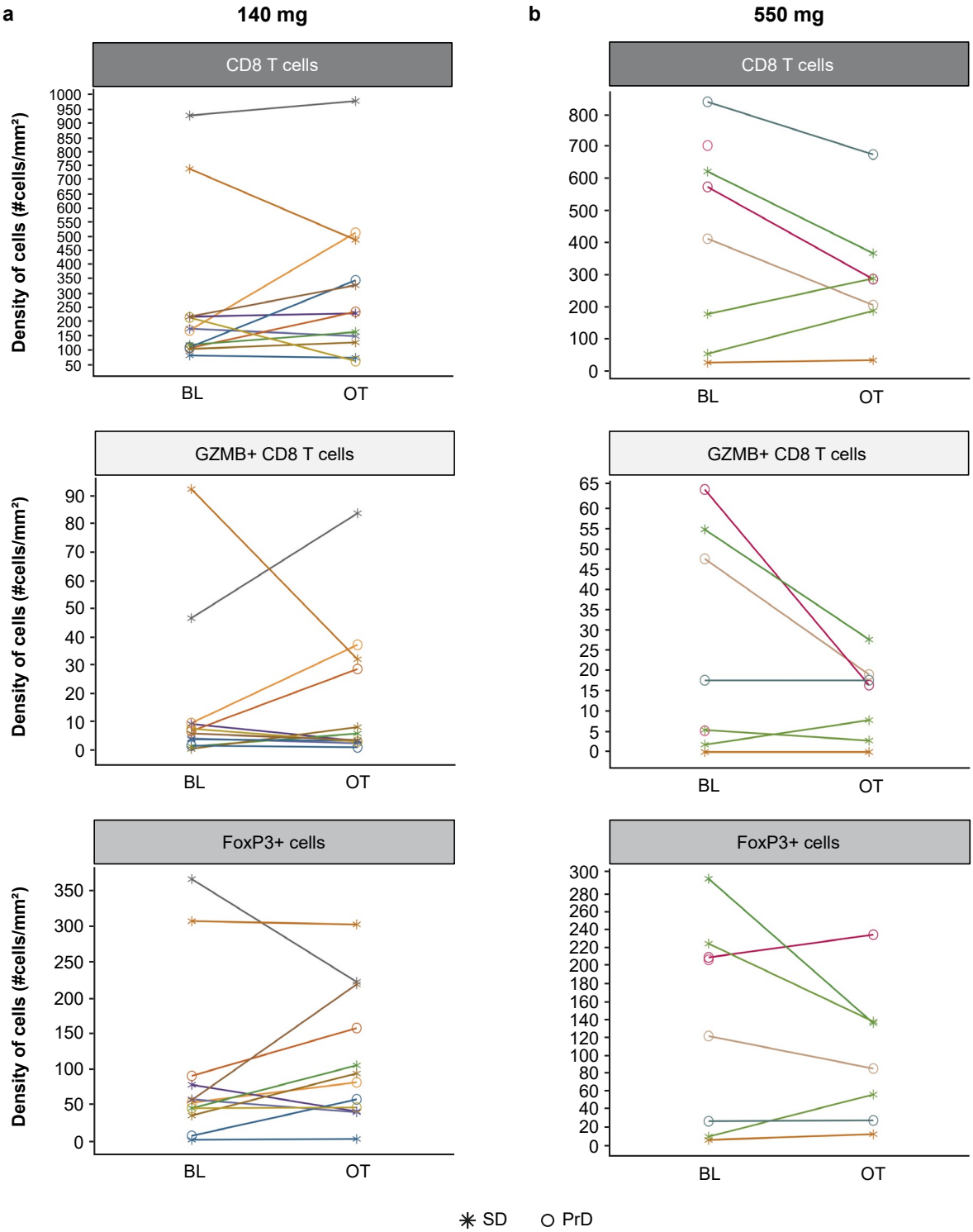

Extended Data Fig. 6 | Infiltration and activation status of CD8 T cells (total cell density) and CD8 T cells positive for granzyme B as well as FoxP3+ cell regulatory T cells analyzed by IHC on BL and OT paired tissue biopsies from individual patients dosed at 140 mg (a) or 550 mg (b). Density is given as the number of cells/mm^2 tissue. Unconnected data points: paired sample did not meet quality check criteria. Labels indicate patient RECIST 1.1 BOR. Unconnected data points: paired sample did not meet quality check criteria and was not included in the analysis. BL, baseline; BOR, best overall response; GZMB, Granzyme B; IHC, immunohistochemistry; OT, on-treatment; pt, patient; SD, stable disease; PrD, progressive disease.

https://doi.org/10.1038/s43018-026-01157-8

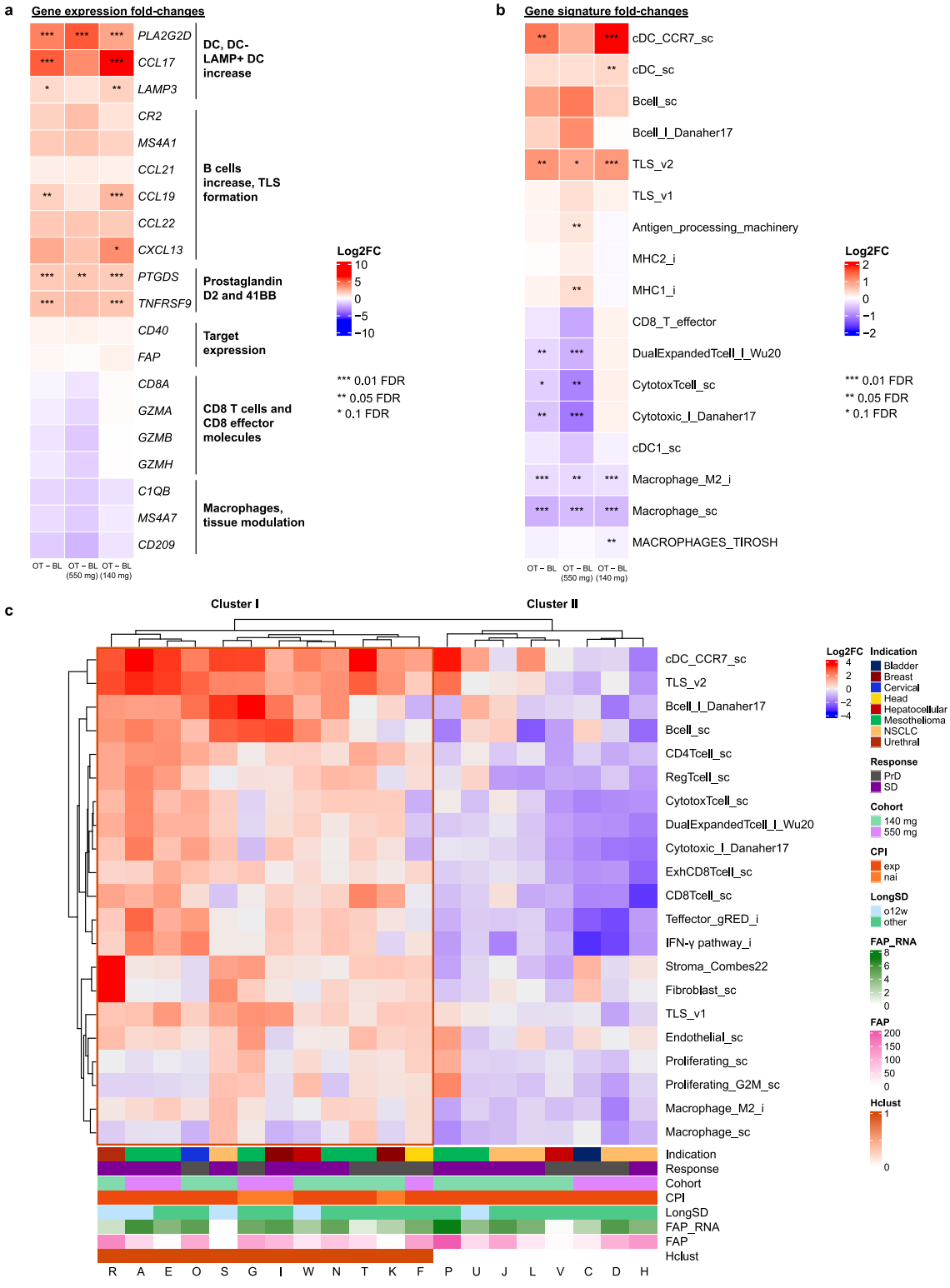

	Odds Ratio	95% CI	*p*-value
CPI	>10^6	0–NA	0.99
FAP	0.1	0.98–1.01	0.39
Arm 550 mg	1.2	0.33–4.51	0.79
Indication NSCLC	0.09	0.01–0.45	0.01
Response (long SD)	1.19	0.33–4.51	0.79

Extended Data Fig. 7 | See next page for caption.

https://doi.org/10.1038/s43018-026-01157-8

Extended Data Fig. 7 | RNA-Seq analysis of macro-dissected, paired biopsy tissues. Gene expression changes are visualized as heatmaps with the color corresponding to Log2FC of OT versus BL. All patients with paired biopsies from the backfill cohorts were included in this analysis, except for three samples which did not pass QC, see Table S5 for details. Number of evaluable paired biopsies tested: $n = 20$; 140 mg cohort $n = 12$; 550 mg cohort $n = 8$. OT-BL: Fold changes estimated across patients from both cohorts, or the 550 mg or 140 mg cohort, respectively. **a**, Aggregated Log2FC for selected genes, grouped and annotated by function. **b**, Aggregated Log2FC for selected gene signatures obtained from the public domain (see Methods and Table S9). **c**, Hierarchical clustering of signature Log2FC at patient level enables associations of gene expression changes with clinical and biomarker parameters. Overview of Log2FC OT versus BL for all individual patients (columns) and selected gene signatures (rows) as well as clinical parameters – response, SD for ≥12 weeks (Long SD), dose group, prior CPI status (naïve vs experienced), FAP expression at baseline (FAP – based on IHC, FAP_RNA – based on RNA-seq) and indication. Samples are hierarchically clustered, and the Hclust highlighted. Table below the hierarchical clustering (Extended Data Fig. 7c): logistic regression analysis for the association between the predictor variables CPI, FAP positivity, dose and indication (NSCLC or other indication) and the dose level and the cluster membership. We also show the association between cluster assignment and response in a logistic regression model predicting response based upon the clustering. Wald test statistics and corresponding p-values assess the significance of each predictor variable. Cluster II includes only experienced patients, thus rendering the logistic regression unestimable for CPI, with unrealistic odds ratio. There was no statistically significant association between cluster assignment and response in a logistic regression model ($p > 0.1$) predicting response based upon the clustering. BL, baseline; CPI, checkpoint inhibitors; FDR, false discovery rate; Log2FC, Log2 fold changes; OT, on-treatment.

https://doi.org/10.1038/s43018-026-01157-8

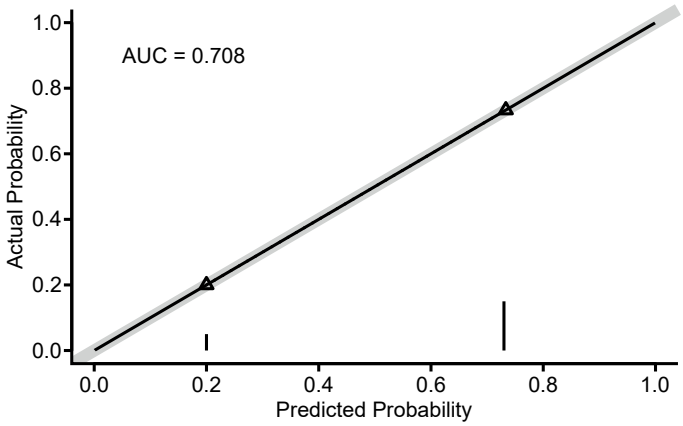

Extended Data Fig. 8 | Calibration plot for logistic regression model predicting Cluster II membership based on NSCLC indication. To evaluate the reliability of the model predicting Cluster II membership based on NSCLC status, we assessed calibration using a calibration plot. The model showed good agreement between predicted probabilities and observed outcomes. X-axis: the predicted probability of being in Cluster II. Y axis: actual observed frequency of membership to cluster II. Predicted probabilities ranged from 0.2 to 0.73, aligning well with observed frequencies. The diagonal line represents perfect calibration. The model showed good calibration, with an area under the ROC curve (AUC) of 0.71, indicating reasonable discriminatory ability and calibration. Shaded area indicates 95% confidence interval from 1,000 bootstrap resamples.

https://doi.org/10.1038/s43018-026-01157-8

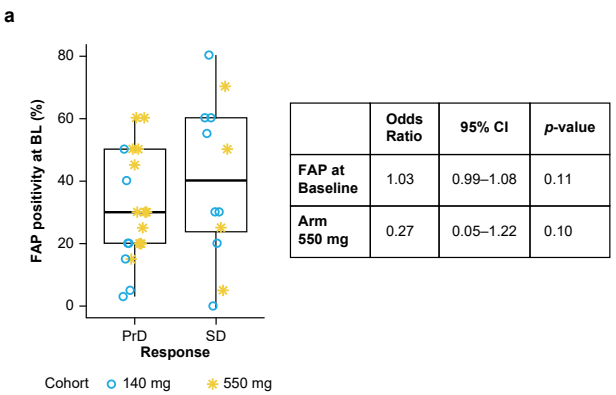

	Odds Ratio	95% CI	*p*-value
FAP at Baseline	1.03	0.99–1.08	0.11
Arm 550 mg	0.27	0.05–1.22	0.10

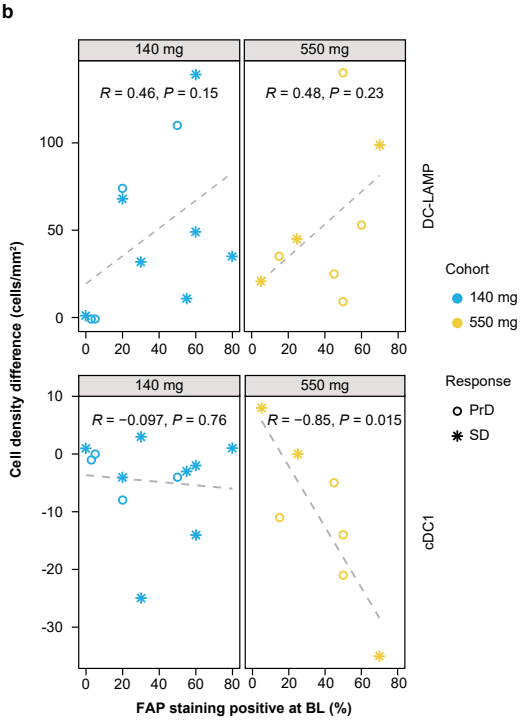

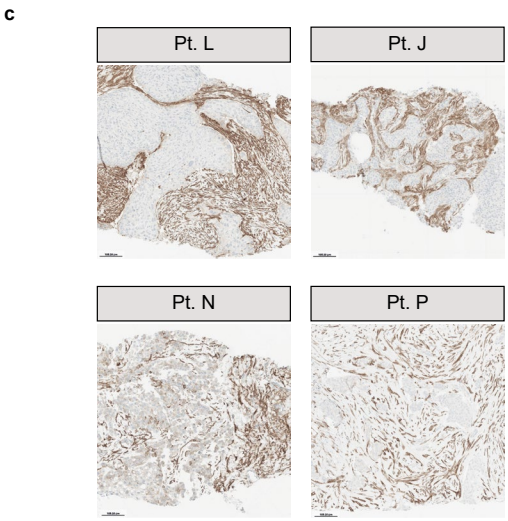

Extended Data Fig. 9 | Correlation of FAP expression with response and PD effects. a, Baseline FAP expression and correlation with response-comparable FAP expression. FAP expression levels (% FAP-positive stroma) were analyzed by IHC in BL tumor tissues. Interpretation of odds ratio estimates: similar FAP positivity values at baseline for PrD and SD response status. Backfill cohorts' patients with at least one response assessment were used. Three patients were removed from the analysis as biopsy samples did not pass the quality check, see Table S5 for details ($n = 27$). The lower and upper hinges of the box plot correspond to the first and third quartiles (the 25th and 75 percentiles). The middle bold line represents the median. The upper whisker extends from the hinge to the largest value no further than 1.5 x IQR from the hinge. The lower whisker extends from the hinge to the smallest value at most 1.5 x IQR of the hinge. Slightly greater median value for BOR = SD. **Table**, Logistic regression analysis for the association between the predictor variables FAP positivity at baseline and the dose level, and the binary outcome variable or response status (PrD or SD). Wald test statistics and corresponding *p*-values assess the significance of each predictor variable. **b**, FAP positivity of BL tissues assessed by IHC was correlated with the magnitude of the response of mature DC-LAMP + DC or cDC1, analyzed by multiplex-IF, in paired tumor tissue biopsies. The difference in OT − BL cell density is depicted on the y axis. Gray dashed line indicates the expected cell density difference using a linear regression model with predictor variables being the FAP positivity at BL. The Pearson correlation coefficient ® and its significance status (two-sided *p*-value) is indicated in the top of each subplot. Patients in the backfill cohorts with two DC-LAMP measurements at BL and OT. Four patients were removed from the analysis as samples did not pass the quality check, see Table S5 for details (total $n = 19$). **c**, Representative IHC images of FAP-positive cells in the tumor region (epithelium and stroma) of BL samples, showing a purely stromal staining pattern (patient IDs L and J) or a mixed pattern (patient IDs N and P), at 10x magnification. BL, baseline; BOR, best overall response; cCD1, cDC1, conventional type 1 DCs; CI, confidence interval; DC-LAMP + DC, DC-lysosomal associated membrane protein-positive dendritic cell; FAP, fibroblast activation protein; OT, on-treatment; PrD, progressive disease; SD, stable disease.

nature portfolio

Corresponding author(s): Bernhard Reis

Last updated by author(s): 13 February 2026

Reporting Summary

Nature Portfolio wishes to improve the reproducibility of the work that we publish. This form provides structure for consistency and transparency in reporting. For further information on Nature Portfolio policies, see our Editorial Policies and the Editorial Policy Checklist.

Statistics

For all statistical analyses, confirm that the following items are present in the figure legend, table legend, main text, or Methods section.

n/a	Confirmed
☐	☒ The exact sample size (*n*) for each experimental group/condition, given as a discrete number and unit of measurement
☐	☒ A statement on whether measurements were taken from distinct samples or whether the same sample was measured repeatedly
☐	☒ The statistical test(s) used AND whether they are one- or two-sided *Only common tests should be described solely by name; describe more complex techniques in the Methods section.*
☐	☒ A description of all covariates tested
☐	☒ A description of any assumptions or corrections, such as tests of normality and adjustment for multiple comparisons
☐	☒ A full description of the statistical parameters including central tendency (e.g. means) or other basic estimates (e.g. regression coefficient) AND variation (e.g. standard deviation) or associated estimates of uncertainty (e.g. confidence intervals)
☐	☒ For null hypothesis testing, the test statistic (e.g. *F*, *t*, *r*) with confidence intervals, effect sizes, degrees of freedom and *P* value noted *Give P values as exact values whenever suitable.*
☒	☐ For Bayesian analysis, information on the choice of priors and Markov chain Monte Carlo settings
☒	☐ For hierarchical and complex designs, identification of the appropriate level for tests and full reporting of outcomes
☐	☒ Estimates of effect sizes (e.g. Cohen's *d*, Pearson's *r*), indicating how they were calculated

Our web collection on statistics for biologists contains articles on many of the points above.

Software and code

Policy information about availability of computer code

Data collection	No custom computer code or algorithms were used in data collection.
Data analysis	No custom computer code or algorithms were used in data analysis. All analyses were performed in the R programming environment.

For manuscripts utilizing custom algorithms or software that are central to the research but not yet described in published literature, software must be made available to editors and reviewers. We strongly encourage code deposition in a community repository (e.g. GitHub). See the Nature Portfolio guidelines for submitting code & software for further information.

Data

Policy information about availability of data

All manuscripts must include a data availability statement. This statement should provide the following information, where applicable:

- Accession codes, unique identifiers, or web links for publicly available datasets
- A description of any restrictions on data availability
- For clinical datasets or third party data, please ensure that the statement adheres to our policy

For eligible studies, qualified researchers may request access to individual patient level clinical data through a data request platform. At the time of writing, this request platform is Vivli (https://vivli.org/ourmember/roche/). For up-to-date information on Roche's Global Policy on the Sharing of Clinical Information and how to request access to related clinical study documents, see here: https://go.roche.com/data_sharing. Source data for all main figures and extended data figures have been provided as source data files. All other data supporting the findings of this study, along with model specifications, files and qualification, including final

modeling parameters, are available from the corresponding author on reasonable request. RNA sequencing data cannot be made available due to regional secondary data use restrictions, data privacy and subject re-identification risks. Medical imaging data (DICOM images) are considered sensitive personal health information (PHI) and there is currently no safe environment for sharing this kind of PHI. Anonymized records for individual patients across more than one data source external to Roche cannot, and should not, be linked due to a potential increase in risk of patient re-identification.

Research involving human participants, their data, or biological material

Policy information about studies with human participants or human data. See also policy information about sex, gender (identity/presentation), and sexual orientation and race, ethnicity and racism.

Reporting on sex and gender	Demographic data included self-reported sex (Table 1). Stratification or analysis by self-reported sex was not performed.
Reporting on race, ethnicity, or other socially relevant groupings	Demographic data included self-reported race/ethnicity (data not presented). Stratification or analysis by self-reported race/ethnicity was not performed.
Population characteristics	Demographic data are presented in Table 1.
Recruitment	Eighty patients with advanced and/or metastatic solid tumors were enrolled across 10 sites within five countries. Participants were identified for potential recruitment by the local investigators using pre-screening enrollment logs and institutional databases.
Ethics oversight	The design and conduct of study WP42627 (NCT04857138) and the imaging substudy WP42627/IMG (conducted at a single site in Spain) complied with all relevant regulations regarding the use of human study participants and were conducted in accordance with the criteria set by the Declaration of Helsinki. The studies were approved by the Institutional Review Boards and/or local Ethics Committees of the participating centers (IRB/EC [CEIC de Navarra: EC_2021/2; HRA & HCRW: 21/FT/0031; De VK Region Hovedstaden: H-21017757; SNUH IRB: H-2104-078-1211; ASM IRB S2021-0747-0001; CPP Ile de France I: CPPIDF1-2022-DI21-cat.1]). The imaging substudy was approved as an amendment to the main study in Spain (CEIC de Navarra: EC_2021/2). All patients provided written informed consent before enrollment and were not compensated for taking part in the study. Human specimen collection and their subsequent evaluations were in accordance with the informed consent agreements.

Note that full information on the approval of the study protocol must also be provided in the manuscript.

Field-specific reporting

Please select the one below that is the best fit for your research. If you are not sure, read the appropriate sections before making your selection.

☒ Life sciences ☐ Behavioural & social sciences ☐ Ecological, evolutionary & environmental sciences

For a reference copy of the document with all sections, see nature.com/documents/nr-reporting-summary-flat.pdf

Life sciences study design

All studies must disclose on these points even when the disclosure is negative.

Sample size	A total of 80 patients were enrolled into the main study (dose-escalation cohorts: n=29; backfill cohorts: n=43) and imaging substudy (n=8). No statistical methods were used to pre-determine sample sizes. Sample sizes for the dose-escalation cohorts were determined by the operating characteristics of the CRM model, as in similar Phase I dose-escalation trials. Sample sizes for the backfill cohorts were determined empirically, with the aim of collecting at least 10 evaluable paired biopsies, which would be sufficient to detect a difference of one standard deviation.
Data exclusions	Patients B, M and Q were excluded from tumor biomarker analysis, as the biopsy samples did not fulfill the QC criteria defined (more details in M&M); For patient L, all DC-LAMP+ values had to be removed due to false detection in this channel. This resulted in a reduction to n=20 or n=19 depending on the analysis, this is detailed in the respective sections/ figure legends.
Replication	Not applicable in view of the first-in-human nature of the study.
Randomization	Not applicable. There was no simultaneous enrollment into several cohorts.
Blinding	Not applicable. The study had an open-label design.

Reporting for specific materials, systems and methods

We require information from authors about some types of materials, experimental systems and methods used in many studies. Here, indicate whether each material, system or method listed is relevant to your study. If you are not sure if a list item applies to your research, read the appropriate section before selecting a response.

Materials & experimental systems

n/a	Involved in the study
☐	☒ Antibodies
☒	☐ Eukaryotic cell lines
☒	☐ Palaeontology and archaeology
☒	☐ Animals and other organisms
☐	☒ Clinical data
☒	☐ Dual use research of concern
☒	☐ Plants

Methods

n/a	Involved in the study
☒	☐ ChIP-seq
☐	☒ Flow cytometry
☒	☐ MRI-based neuroimaging

Antibodies

Antibodies used: All antibody reagents were obtained from commercial suppliers. Manufacturers, clones and catalogue numbers for all antibody reagents have been included in Table S4, S5, S7 and S8. All biomarker data were generated applying appropriately qualified/validated standard operating procedures and/or methods, including the use of specific and appropriately diluted antibody reagents. Qualification or validation reports can be made available upon request.

Validation: Methods for the assessment of RO and TBNK+Monocytes were developed, validated and executed at Q Squared Solutions, a qualified and certified CROaccording to Good Clinical Practice Guidelines. Validation reports can be made available upon request.

Clinical data

Policy information about clinical studies

All manuscripts should comply with the ICMJE guidelines for publication of clinical research and a completed CONSORT checklist must be included with all submissions.

Clinical trial registration: NCT04857138 (EudraCT: 2020-004489-21)

Study protocol: A redacted version of the protocol has been provided with the submission

Data collection: Eighty patients with advanced and/or metastatic solid tumors were enrolled between May 2021 and January 2023 at 10 centers in five countries.

Outcomes: The primary objective of the study was evaluation of RO7300490 safety and tolerability. Secondary objectives were assessment of pharmacokinetics,immunogenicity, and anti-tumor activity. Pharmacodynamics were assessed as an exploratory objective. Outcome measures for all objectives are described indetail in the Methods section.

Plants

Seed stocks: *Report on the source of all seed stocks or other plant material used. If applicable, state the seed stock centre and catalogue number. If plant specimens were collected from the field, describe the collection location, date and sampling procedures.*

Novel plant genotypes: *Describe the methods by which all novel plant genotypes were produced. This includes those generated by transgenic approaches, gene editing, chemical/radiation-based mutagenesis and hybridization. For transgenic lines, describe the transformation method, the number of independent lines analyzed and the generation upon which experiments were performed. For gene-edited lines, describe the editor used, the endogenous sequence targeted for editing, the targeting guide RNA sequence (if applicable) and how the editor was applied.*

Authentication: *Describe any authentication procedures for each seed stock used or novel genotype generated. Describe any experiments used to assess the effect of a mutation and, where applicable, how potential secondary effects (e.g. second site T-DNA insertions, mosiacism, off-target gene editing) were examined.*

Flow Cytometry

Plots

Confirm that:

☐ The axis labels state the marker and fluorochrome used (e.g. CD4-FITC).

☐ The axis scales are clearly visible. Include numbers along axes only for bottom left plot of group (a 'group' is an analysis of identical markers).

☐ All plots are contour plots with outliers or pseudocolor plots.

☐ A numerical value for number of cells or percentage (with statistics) is provided.

Methodology

Sample preparation	Blood samples were collected in Sodium Heparin Blood Collection Tubes (BD Biosciences) at the sites and sent at ambient temperature for sample preparation and flow cytometry analysis according to validated assay protocols. All incubation steps were conducted at room temperature up to and including the cell lysis stage, and at 4°C thereafter. Anti-coagulated whole blood (100 µL) was transferred to each assay tube. The saturation tube was incubated for one hour with the drug. Cells were lysed with BD Pharm Lyse (BD Biosciences) to remove red blood cells. Cells were washed in phosphate-buffered saline (PBS), blocked with FCR blocking (Miltenyi Biotec) andstained with the appropriate antibody cocktail mixture. Cells were washed and resuspended in PBS before acquisition.
Instrument	Data acquisition for the CD40 RO assay was conducted using FACS Canto II (10 color, 3 laser) instruments (BD Biosciences). Data acquisition for the phenotyping assay was conducted using FACS Canto II (8 color, 3 laser) instruments (BD Biosciences).
Software	Analysis was carried out using FACSDiva (BD Biosciences) acquisition templates specific to each assay and FACSDiva software.
Cell population abundance	The percentage of RO on B cells and monocytes are calculated using the following equation: RO calculation of MFI values % RO = ((MFI bound-MFI Ctrl)/(MFI total-MFI Ctrl)) * 100
Gating strategy	The gating strategies of the two assays used are summarised in the Methods.

☐ Tick this box to confirm that a figure exemplifying the gating strategy is provided in the Supplementary Information.